THE ASTROPHYSICAL JOURNAL, 330:634–660, 1988 July 15

VIRGO DWARFS: NEW LIGHT ON FAINT GALAXIES

CHRIS IMPEY
Steward Observatory, University of Arizona
GREG BOTHUN
Astronomy Department, University of Michigan
AND
DAVID MALIN
Anglo-Australian Observatory
Received 1987 October 20; accepted 1988 January 8

ABSTRACT

A sample of 137 low surface brightness galaxies in the Virgo Cluster has been studied, with initial selection on photographically amplified UK Schmidt plates. The limiting isophote for galaxy detection is $\mu_B \approx 27$ mag arcsec^{-2}. There is substantial overlap with existing catalogs of Virgo dwarf galaxies, but the 27 new galaxies have unusually low surface brightness and large angular size. The first of the new galaxies to have a redshift turns out to be the largest, most gas-rich spiral known, located far beyond the Virgo Cluster. However, most appear to be dwarf elliptical galaxies. H I observations show the low surface brightness galaxies to be gas-poor, with $M_{\rm H\,I} < 3\text{–}5 \times 10^6\ M_\odot$. CCD images are used to derive surface photometry for 26 objects, and the radial profiles are generally well fitted by an exponential. The colors are unusually blue for ellipticals, implying low metallicity and relatively youthful ages. The star formation history that can lead to galaxies with such blue stars and such low surface mass densities is unknown.

The relationships between the structural parameters of dwarf galaxies are discussed, with an emphasis on the selection effects imposed by the brightness of the night sky. The relationship between surface brightness and luminosity breaks down at $M_B \approx -16$, and the range of central surface brightness for a given luminosity can be over 5 mag. Our understanding of the intrinsic distribution of dwarf structural parameters is heavily obscured by selection effects. Any survey tends to choose galaxies of a luminosity and surface brightness that give the maximum angular size on the discovery plate. There may be large populations of galaxies with extremely low surface brightness. Low-luminosity galaxies do not tend to have the bright nuclei that aid their discovery and a number of low-luminosity galaxies have flat cores. The effect of this uncertainty on the luminosity function of dwarf ellipticals (and similarly, all faint galaxies) is dramatic. In particular, a divergent exponential tail to the galaxy luminosity function cannot be ruled out.

Subject headings: galaxies: clustering — galaxies: photometry — galaxies: redshifts — galaxies: stellar content — galaxies: structure — radio sources: galaxies — radio sources: 21 cm radiation

I. INTRODUCTION

The humble dwarf galaxy is one of the most interesting objects in the universe. Most examples of these galaxies have low luminosity ($M_B > -16$), and a surface brightness below the level of the night sky. Despite their unassuming appearance, dwarf galaxies may hold the key to many questions of galaxy formation, structure, and evolution. Dwarfs are expected to trace the mass in hierarchical theories of galaxy formation (Dekel and Silk 1986), and they may be responsible for the copious low-metallicity absorption seen in the spectra of high-redshift quasars (Ikeuchi and Norman 1987). If mass-to-light ratios are as high as those seen in the Local Group dwarf spheroidals, then dwarf galaxies could form a major mass component in the universe. The observed relationships between structural parameters for dwarfs have been used to constrain theories for the structure and evolution of low mass galaxies. However, all of these theoretical investigations are limited by our incomplete knowledge of the properties of low luminosity galaxies.

Most data on dwarf galaxies have come from studies of the Virgo Cluster (Caldwell 1983; Binggeli, Sandage, and Tarenghi 1984, 1985; Bothun *et al.* 1986; Ichikawa, Wakamatsu, and Okamura 1986), and more recently the Fornax cluster (Caldwell and Bothun 1987). In particular, the massive survey of the Virgo Cluster by Sandage and co-workers has defined the luminosity function of dwarfs down to $M_B \approx -12$. We will concentrate on dwarf ellipticals, because they dominate the luminosity function fainter than $M_B \approx -16$ (Sandage, Binggeli, and Tammann 1985). The following properties of dwarf ellipticals seem well established. They show a strong dependence of both isophotal surface brightness and radius on absolute luminosity. The radial profiles are well fitted by an exponential, but unlike the disk galaxies that are also fitted by exponentials, dwarf ellipticals are usually round. The fraction of nucleated galaxies falls with decreasing luminosity, and the nucleated dwarfs have the reddest optical colors. The colors of dE's indicate metallicities similar to metal-rich Galactic globular clusters, $-1 < [\mathrm{Fe/H}] < -0.5$. Dwarf ellipticals appear to be distinct from dwarf irregulars and more luminous ellipticals. In particular, the low H I limits for dE's and the lack of a well-defined color versus surface brightness relation make it unlikely that dwarf ellipticals are faded remnants of dwarf irregulars (Bothun *et al.* 1986). There is no smooth continuity between dE's and giant ellipticals either in terms of core parameters (Kormendy 1985) or the shape of the luminosity function (Sandage, Binggeli, and Tammann 1985). We note that the spatial distribution of dE's, in the Virgo Cluster at any rate, closely follows the distribution of luminous early-type cluster members (Binggeli, Tammann, and Sandage 1987). The luminosity function is well fitted by a Schechter (1976) function, logarithmic at bright magnitudes and exponential at faint magnitudes.

Many aspects of dwarf galaxies are poorly understood. Few of the lowest luminosity galaxies have redshifts, since few of them have nuclei and the surface brightness is often too low for spectroscopy. Therefore the assignment to Virgo or Fornax membership is based on structural parameters and must be considered uncertain. The range of metallicities and ages of the stellar populations are also poorly known. The nature of the nuclei is unclear, though they have similar spectra to metal-rich Galactic globular clusters. Finally, the detailed spatial distribution of low-luminosity galaxies has yet to be defined. In both the Virgo and Fornax clusters, there is evidence that the dwarfs have a larger velocity dispersion than the more luminous galaxies (Bothun and Mould 1988). But the space distribution of dwarfs outside of clusters is unknown. Therefore it is unclear whether the dwarfs arise as the detritus of galaxy interactions in rich environments, or as tracers of density fluctuations in the early universe.

Perhaps the most important area of ignorance, and one that has been unjustly neglected, is the effect of galaxy selection techniques on our understanding of galaxy properties. The ultimate barrier to the detection of faint galaxies is the brightness of the night sky. Selection effects are imposed by the combined glow of the Milky Way, the zodiacal light, and atmospheric luminescence. Disney (1980) has described it vividly: "We are like prisoners in a lighted cell trying to discern our whereabouts by peering out through a small casement into the darkness outside. We can see the steet lamps easily enough, and the lighted windows, but can we see or correctly infer the houses and the trees?" The effect of surface brightness on observed galaxy properties and on the selection of those galaxies has a long history. Hubble (1936) found a Gaussian shape of the galaxy luminosity function because he was almost entirely restricted to high surface brightness galaxies. Zwicky (1942) correctly guessed that the luminosity function became an exponential at faint magnitudes. Arp (1965) pointed out that extended objects will not uniformly fill a plane of apparent luminosity versus apparent diameter but will lie in a broad band. Surface photometry of the disks of bright spirals (Freeman 1970) showed that the central surface brightness has a remarkably narrow distribution. Disney (1976) and Allen and Shu (1979) have accounted for the narrow range of central surface brightness in terms of selection effects. At a given luminosity, large galaxies have a central surface brightness that dips below the night sky threshold, and small galaxies with bright cores are difficult to resolve and distinguish from stars. Both extremes of surface brightness are underrepresented. In fact, any galaxy selected photographically will tend to have the central surface brightness that gives it the largest isophotal diameter at the limit of the plate material (Disney 1980).

Electronic detectors have dramatically improved the prospect of imaging galaxies fainter than the night sky. On a dark site with a medium sized telescope, surface photometry of galaxies with central surface brightness less than 5% of the night sky is possible. Yet the continuing power of photography as a discovery medium cannot be overstated. The uniformity and information density of fine grain emulsions over a large field is not rivaled by electronic detectors. In this paper we describe galaxies in the Virgo Cluster selected from material derived by a photographic amplification technique from deep plates taken with the UK Schmidt telescope. In § II, the plate material is described and the overlap with previous surveys is discussed. Follow up observations consisting of multicolor surface photometry and H I measurements are described in § III. The colors of dwarf galaxies are interpreted in terms of stellar populations and ages in § IV. Structural properties are reviewed in § V, with an emphasis on selection effects. The luminosity function of dwarf galaxies and uncertainties in its determination are discussed in § VI. Conclusions follow in § VII.

II. SELECTION OF LOW SURFACE BRIGHTNESS GALAXIES

a) *Photographic Amplification*

The sample of low surface brightness (LSB) galaxies used in this study was found by visual inspection of high-contrast copies of UK Schmidt plates. These were made by combining photographically amplified derivatives (Malin 1978) obtained several years ago from three deep plates of the Virgo Cluster which were taken for other projects. All the original exposures were made in dark conditions on hypersensitized Eastman Kodak IIIa-J emulsion behind a GG 395 Schott glass filter. The plate data are shown in Table 1.

Contact copies of each of the three original plates were made on Agfa-Gevaert Fo 710 sheet film using a diffuse-light contact copier. The copy exposure was selected so that the developed density in the sky region of each of the high-contrast copy positives was very low (see Malin 1981). Images of selected areas from each of the three films were superposed in register by enlargement onto 8×10 inch (20×25 cm) sheets of Kodak Kodalith Film Type 2556 with the individual exposures adjusted so that each positive contributed equally to the resulting negative. To ensure precise registration, the film was held in the superposition frame illustrated in Malin and Murdin (1984). The enlargement factor was about 4 and each field covered a little less than $2° \times 2\overset{\circ}{.}1$ of sky at an image scale of about 15″ mm^{-1}. A fuller description of multiple-image superposition has been published elsewhere (Malin 1987).

The existence of three similar but separate high-contrast copies prior to photographic superposition gave us two important advantages. Dust spots on the back of the original plates or on the platen of the contact printer can produce images similar to those we were interested in, so the reality of each of the LSB galaxies we selected from the combined negative was confirmed by ensuring that it appeared on more than one of the enhanced film positives. Most of the fainter galaxies in our sample were too faint to be confirmed by inspection of the original plates, even if they had been available. The second major advantage of combining the positives from several plates is the dramatic improvement in the signal-to-noise ratio which is obtained in the superposed image, which of course is in the

TABLE 1

PLATE DATA

Plate Number	Center (γ, δ:1950)	Exposure Time (minutes)	Date
J2137.........	$12^h27\overset{m}{.}0$, $+13°30'$	70	1976 Mar 28
J2934.........	12 25.0, +13 20	64	1977 Feb 20
J3209.........	12 25.0, +13 20	32	1977 May 22

form of a negative, ideally suited for visual faint object detection.

The faintest galaxies in the sample were selected because their images on the high-contrast negative films were unsaturated; indeed, many of them attract attention because they had a luminosity distribution which is unusually flat. The selection of unsaturated images immediately eliminates confusion between background normal ellipticals and many LS galaxies. Those extended objects which are saturated on the composite negative film are then compared with conventional, low-contrast copies of the best of the original plates (J2137) to see if they had luminosity profiles typical of background objects. This selection procedure would naturally select against those dwarf galaxies (if any) which have luminosity profiles like their giant counterparts but were only a fraction the angular size. The presence or absence of nuclei did not strongly influence the selection of galaxies for this sample.

b) Low Surface Brightness Galaxies

Films of the nine Virgo fields covering 7.7 deg^2 were examined for large angular size and low surface brightness galaxies. In particular, selection was limited to image diameters of greater than approximately 30″ at the limiting isophote. Since initial selection was by visual inspection, this sample is not rigorously defined by angular diameter. Nor was homogeneous selection by central surface brightness possible due to the vagaries of visual inspection and the saturated galaxy cores produced by the increased contrast of the amplification process. Bright galaxies with dense cores were avoided, and the sample should be biased towards large angular size and low central surface brightness.

The 137 galaxies selected are listed in Table 2. The positions were determined by astrometry of the film derivatives using the two-axis Grant machine at Kitt Peak. The number of primary positional references available in each field was limited, but the final accuracy should be less than 10″ in each coordinate. Columns (1) and (2) give the running number within our fields and the VCC number from the Binggeli, Sandage, and Tammann atlas (1985, hereafter BST85). The positions for epoch 1950 are in columns (3) and (4). Positions of galaxies in common agree with those listed in BST85. Column (5) has the angular diameter in arcseconds at the limiting isophote of the UK Schmidt photographic material. Galaxies marked with daggers are interesting for further study because either they are new, they have large angular size, $D_{27} > 100''$, or the ratio of D_{27} to $D_{25.5}$ (from BST85) is greater than 2, indicating a large scale length. Column (6) shows the galaxies with CCD photometry or H I measurements in this paper. The limit of the amplification technique is determined by comparing the maximum diameter on the plate with the isophotal diameter determined from CCD surface photometry. For 21 galaxies, we find a limiting surface brightness in mag arcsec^{-2} of $(\mu_{\rm lim})_B = 27.2 \pm 0.7$. The amplified plate material reaches an impressive limiting detection isophote of less than 1% of the brightness of the night sky.

There is considerable overlap with the BST85 atlas in Table 2. Only 20% of the low surface brightness galaxies in Table 2 have no counterpart in the Virgo atlas. Figure 1 shows the limiting diameters from BST85 plotted against those from this work. The estimates of angular size in each survey are only accurate to 10%–15%, giving considerable scatter. The deeper limiting isophote of the UK Schmidt material gives image sizes larger by 50% on average. There is also a tendency for the faintest galaxies to have the largest ratios of $D_{27.2}$ to $D_{25.5}$. Cases where $D_{27.2}$ is less than $D_{25.5}$ are mostly due to the errors in measuring image diameters. The new survey has uncovered 27 new galaxies, and they are of interest because of the large ratios of $D_{27.2}/D_{25.5}$, implying large scale lengths and values of central surface brightness low enough to avoid detection at $\mu_B = 25.5$. The surface density of newly discovered LSB galaxies is 3.5 per square degree, compared with 25 galaxies per square degree in the same region of the BST85 atlas. Over 300 of these extreme LSB galaxies can be detected in the entire Virgo Cluster. The histogram of $D_{27.2}$ for the newly identified galaxies is shown at the bottom of Figure 1. The distribution of $D_{27.2}$ for the new galaxies is similar to that of the sample as a whole, so we infer that there must be many more galaxies of large angular size but with a mean surface brightness below the limit of the amplified photographs. The Virgo membership of the new low surface brightness galaxies of large angular size is highly probable, by the morphological arguments given in BST85. However, it is very disconcerting that one of the largest angular size galaxies (V1L3), and the first for which we have a redshift, turns out to be well beyond Virgo at 25,000 km s^{-1} (Bothun *et al.* 1987).

We can draw an important conclusion from the detection of low surface brightness galaxies on amplified photographic plates. Galaxies as faint as $B_{\rm tot} \approx 20$, with central surface brightness as low as $\mu_B \approx 26$ can be selected down to a limiting isophote of $\mu_B \approx 27$ using UK Schmidt plate material. Large telescopes and large plate scales are not necessary to study low surface brightness galaxies. We note that much of the southern sky has the three or more high-quality UK Schmidt plates that are necessary for photographic coaddition and amplification. The second Palomar sky survey is now underway and will provide similar plate material in the north. The amplification technique described above can therefore be used to define large new samples of faint galaxies, using big telescopes only for calibration and to follow up the most interesting cases.

III. SURFACE PHOTOMETRY, COLORS, AND H I CONTENT

a) CCD Photometry

An RCA 320 × 512 CCD was used to take images of 33 galaxies from the list in Table 2. The subset of galaxies with CCD data was chosen to be broadly representative of the whole sample. The observations were made during 1985 February 5–9 and April 10–16 on the 100 inch (2.54 m) DuPont telescope at Las Campanas Observatory in Chile. The detector was used in direct imaging mode without any transfer optics, giving a plate scale of 0″.34 pixel.$^{-1}$ Exposures were made through Johnson B and V filters and a Cousins I filter. Standard stars from the list of Kent (1985) were used for a primary calibration, and color equations were derived for each filter. In our comparison with other data we have converted published colors into our hybrid color system, noting that $(V-I)_{\rm Cousins} = 0.78(V-I)_{\rm Johnson}$. The RCA chip had a readout noise of ~ 35 electrons during the observations, but the exposures were long enough that noise from the night sky emission dominates in every waveband. Exposure times of 1800 (B), 600 (V), and 900 (I) s were used in February and exposure times in April were 900 (B), 1200 (V), and 600 (I) s. The raw frames were corrected for the bias level contained in the overscan columns of the RCA chip, and flat-fielding was accomplished with twilight exposures. Dome flats were also taken, but the best results were obtained using the twilight sky. The reduced frames are

TABLE 2

Low Surface Brightness Galaxies

Galaxy	VCC	R.A.	Dec	D_{27}	CCD	HI
		(^{h} ^{m} ^{s})	(° ′ ″)	(arcsec)		
(1)	(2)	(3)	(4)	(5)	(6)	
V1L1	1656	12 33 42.5	+14 56 40	48	√	√
V1L2	1590	12 32 24.0	+14 55 27	34		
V1L3	...	12 34 28.1	+14 36 19	113†	√	√
V1L4	1582	12 32 11.3	+14 29 56	57	√	√
V1L5	1702	12 34 35.7	+14 15 30	79	√	√
V1L6	1616	12 32 57.1	+14 32 11	53		
V1L7	1604	12 32 39.4	+14 15 45	53		
V1L8	1495	12 30 46.5	+14 12 40	45		
V1L9	...	12 34 02.3	+14 55 49	29†		
V1L10	...	12 33 33.2	+14 54 22	26†		
V1L11	...	12 31 54.2	+14 45 43	50†		
V1L12	...	12 32 25.2	+14 40 59	25†		
V1L13	1682	12 34 05.6	+14 30 05	53†		
V1L14	...	12 33 12.6	+14 21 14	59†		
V1L15	...	12 33 04.5	+14 21 59	47†		
V2L1	1337	12 28 33.6	+15 20 42	53	√	√
V2L2	1223	12 27 13.0	+15 23 42	56	√	
V2L3	1222	12 27 13.4	+15 18 06	62		
V2L4	1181	12 26 50.6	+15 20 27	72†		
V2L5	...	12 28 24.3	+15 02 56	63†		
V2L6	1274	12 27 45.5	+14 58 47	37		
V2L7	1228	12 27 13.3	+14 54 28	47		√
V2L8	...	12 28 44.7	+14 54 59	67†	√	√
V2L9	1056	12 25 25.4	+14 44 57	51†		
V2L10	1276	12 27 46.6	+14 57 26	24		
V2L11	...	12 28 37.2	+14 52 33	32†		
V2L12	...	12 28 10.3	+14 53 20	37†		
V2L13	1248	12 27 25.8	+14 44 55	24		
V3L1	925	12 24 06.5	+15 21 44	51	√	√
V3L2	812	12 23 03.5	+15 28 18	45		
V3L3	725	12 21 52.7	+15 21 09	103†	√	√
V3L4	668	12 21 15.6	+15 24 12	47		
V3L5	878	12 23 38.6	+15 12 24	53	√	
V3L6	780	12 22 41.6	+15 07 23	41		
V3L7	963	12 24 27.9	+15 03 35	47		
V3L8	1006	12 24 53.7	+14 42 38	43	√	√
V3L9	757	12 22 21.4	+14 55 57	26		
V3L10	748	12 22 15.6	+14 51 14	43		
V3L11	777	12 22 39.5	+14 43 05	40		
V3L12	...	12 22 03.7	+15 26 30	26†		
V3L13	1026	12 25 04.8	+15 07 00	34		
V3L14	795	12 22 51.6	+15 04 49	35		
V3L15	...	12 23 23.3	+14 55 08	35		
V3L16	1029	12 25 07.7	+14 49 10	24		
V4L1	1235	12 29 23.0	+14 34 35	72		
V4L2	...	12 27 18.6	+14 29 39	40†		
V4L3	1194	12 26 58.3	+14 26 40	41		
V4L4	1137	12 26 18.7	+14 26 04	57†		
V4L5	1105	12 25 56.1	+14 25 58	78†	√	√
V4L6	1373	12 29 40.9	+14 20 33	50	√	√
V4L7	1287	12 27 53.3	+14 15 24	111†	√	√
V4L8	1371	12 29 04.1	+14 05 48	73†		
V4L9	1351	12 28 44.8	+14 06 02	104†	√	√
V4L10	...	12 26 14.0	+13 59 51	78†		
V4L11	1301	12 28 05.9	+13 53 34	31†		
V4L12	1214	12 27 07.2	+14 20 00	38†		
V4L13	...	12 28 49.5	+14 09 50	40†		
V4L14	1241	12 27 22.5	+14 13 52	32		
V4L15	1328	12 28 25.2	+13 53 35	26†		
V6L1	1561	12 31 48.6	+13 11 33	79	√	
V6L2	1539	12 31 31.3	+13 01 43	78	√	√
V6L3	1523	12 31 13.1	+13 03 56	37		
V6L4	1517	12 31 06.3	+12 51 23	41		
V6L5	1466	12 30 20.5	+12 54 58	25		
V6L6	1438	12 30 00.1	+12 55 04	75	√	√
V6L7	1418	12 29 37.5	+12 47 07	45		
V6L8	1413	12 29 34.5	+12 42 41	38		√
V6L9	1482	12 30 36.7	+12 33 58	37		
V6L10	1369	12 29 02.0	+12 20 24	54		
V6L11	...	12 29 47.1	+12 35 27	143†		√
V6L12	1518	12 31 07.5	+12 40 04	29		
V6L13	1494	12 30 43.9	+12 33 58	22		
V6L14	...	12 29 46.2	+12 30 56	50†		
V7L1	1298	12 27 59.1	+13 11 03	63†		√
V7L2	...	12 27 53.3	+13 08 34	123†		
V7L3	1149	12 26 24.3	+13 11 15	70	√	√
V7L4	...	12 27 20.2	+12 54 11	45†		
V7L5	1213	12 27 06.0	+12 49 43	78†		
V7L6	...	12 26 35.5	+12 46 33	51†		
V7L7	1123	12 26 09.3	+12 49 38	75		√
V7L8	1259	12 27 33.4	+12 39 32	35		
V7L9	1278	12 27 45.2	+12 31 24	37		
V7L10	1264	12 27 38.6	+12 28 37	70†		
V7L11	1136	12 26 16.9	+12 24 32	50		
V7L12	1162	12 26 33.0	+12 25 55	54†	√	√
V7L13	1157	12 26 28.8	+12 42 48	26		
V7L14	1177	12 26 47.0	+12 39 26	34		
V7L15	1103	12 25 53.6	+12 37 16	35†		
V7L16	1216	12 27 10.2	+12 19 36	44		
V8L1	793	12 22 49.5	+13 20 58	63		
V8L2	779	12 22 41.1	+13 18 16	60†		

TABLE 2.—*Continued*

Galaxy	VCC	R.A. (^{h} ^{m} ^{s})	Dec (° ′ ″)	D_{27} (arcsec)	CCD	HI
(1)	(2)	(3)	(4)	(5)	(6)	
V8L3	1027	12 25 07.4	+13 09 24	70†	√	√
V8L4	930	12 24 09.1	+13 07 23	47		
V8L5	896	12 23 50.5	+13 03 50	59†		
V8L6	800	12 22 56.2	+12 54 55	73†	√	√
V8L7	871	12 23 33.5	+12 50 14	139†		
V8L8	962	12 24 27.1	+12 47 01	79		√
V8L9	803	12 22 56.5	+12 46 19	40		
V8L10	775	12 22 37.2	+12 39 40	37		
V8L11	1052	12 25 24.9	+12 38 36	148†	√	
V8L12	998	12 24 51.2	+12 36 30	63†		
V8L13	927	12 24 06.4	+13 20 59	35†		
V8L14	804	12 22 58.0	+13 15 30	61†		
V8L15	814	12 23 04.4	+13 07 40	44†		
V8L16	1023	12 25 02.5	+13 04 50	44†		
V8L17	923	12 24 04.2	+13 04 50	59†		
V8L18	...	12 25 03.9	+12 54 04	43†		
V8L19	...	12 24 21.4	+12 38 34	65†		
V9L1	1396	12 29 28.3	+12 13 48	59		
V9L2	1216	12 27 13.8	+12 19 17	50		
V9L3	...	12 26 18.0	+12 18 14	40†		
V9L4	1336	12 28 34.8	+12 06 03	63	√	
V9L5	1331	12 28 28.7	+11 58 25	56	√	
V9L6	1366	12 29 00.7	+11 51 50	43		
V9L7	1115	12 26 02.5	+12 01 41	50		
V9L8	1093	12 25 48.3	+11 59 10	66		
V9L9	1212	12 27 08.3	+11 54 27	89	√	
V9L10	1312	12 28 15.7	+11 48 15	28		
V9L11	1291	12 27 53.6	+11 42 24	38		
V9L12	1420	12 29 45.0	+12 19 01	54		
V9L13	1369	12 29 05.9	+12 19 30	50		
V9L14	1335	12 28 36.0	+12 20 32	45†		
V10L1	823	12 23 06.9	+12 35 22	62		
V10L2	...	12 23 00.8	+12 41 34	40†		
V10L3	...	12 21 47.6	+12 36 08	34†		
V10L4	615	12 20 32.2	+12 17 30	86†		√
V10L5	853	12 23 23.5	+12 04 39	29†		
V10L6	752	12 22 15.6	+12 05 43	26		
V10L7	732	12 21 58.5	+12 05 16	34		
V10L8	707	12 21 40.5	+12 02 19	37	√	√
V10L9	705	12 21 38.9	+12 13 26	78		√
V10L10	687	12 21 25.4	+12 10 10	38		
V10L11	728	12 21 53.8	+12 32 16	37†		
V10L12	...	12 21 28.3	+12 13 04	34†	√	
V10L13	840	12 23 14.8	+11 56 20	38	√	
V11L1	1663	12 35 55.0	+12 09 53	59	√	√
V11L2	1601	12 32 35.5	+12 10 30	47	√	√

uniform, with large scale gradients of $<0.5\%$ (B), $<1\%$ (V), and $<2\%$ (I). The average brightness of the moonless sky was $\mu_V = 22$ mag arcsec^{-2}. We note that the dark sky in Chile and the high uniformity of the reduced frames was essential for accurate surface photometry of such faint galaxies.

Surface photometry was accomplished using a modified version of the GASP image analysis package (Cawson 1983), as described by Bothun *et al.* (1986). Of the 33 galaxies selected for CCD measurement, only one was too faint to be visible on the most sensitive (V) picture. One extreme LSB galaxy in the Fornax cluster was also measured, and it will be considered along with the Virgo galaxies. Three galaxies were too faint for surface photometry, but a central surface brightness could be measured. The surface photometry was difficult to perform by usual techniques since the instrinsic S/N of each isophote was generally less than 20. This, combined with the "lumpy" nature of the extremely LSB [i.e. $(\mu_0)_B < 25$] galaxies, often caused the ellipse-fitting routine to terminate prematurely. An

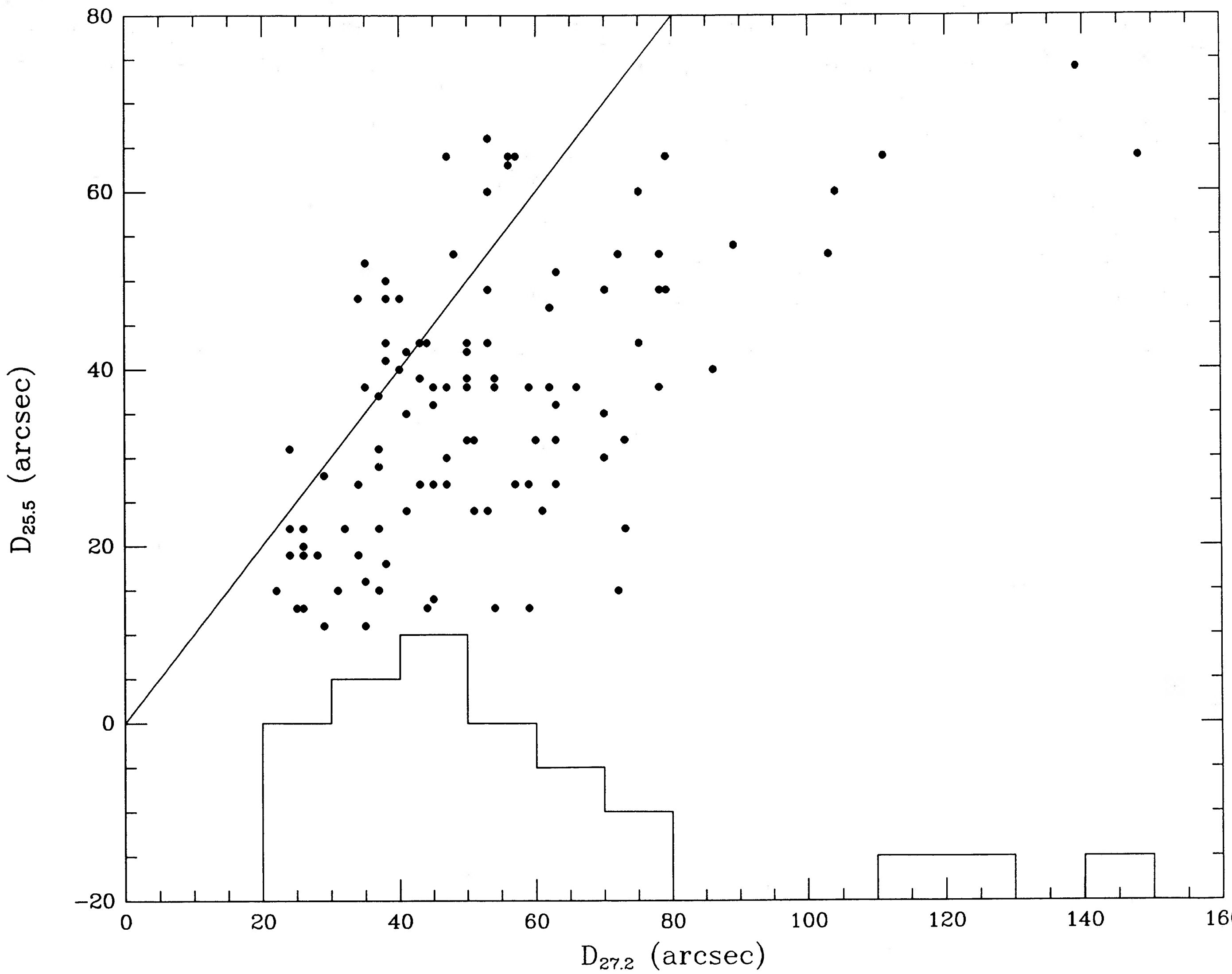

FIG. 1.—The angular diameter ($D_{27.2}$) in arcsec from the survey on photographically amplified Schmidt plates is plotted against the angular diameter ($D_{25.5}$ in arcsec from the Virgo atlas of Binggeli, Sandage, and Tammann 1985). The histogram shows the angular size distribution of the newly discovered galaxies.

iterative procedure was used to mask out blobs not associated with the LSB galaxy, allowing satisfactory ellipses to be fitted to the bulk of the visible galaxy. In addition, the starting radius of the first ellipse was varied with central surface brightness in order that this ellipse could be fitted with sufficient S/N to serve as a starting point for subsequent ellipses. There were often significant changes in the eccentricity or position angle of successive ellipses, changes which actually represent the chaotic structure of some extreme LSB galaxies. It is important to point out that blobs were masked out only when they were not associated with the LSB galaxy (foreground stars, background galaxies). In each case less than 10% of the galaxy area was masked, and the masked area was replaced with the average surface brightness in that annulus. By contrast, the galaxies V3L3, V8L3, and V8L6 are genuinely "lumpy," and the exponential fits to those galaxies are correspondingly poor.

The derived surface brightness profiles for the galaxies which could be fitted with ellipses are shown in Figure 2. In those cases where the light distribution could be adequately represented by an exponential, it is shown as a dashed line. The limiting surface brightness that could be adequately fitted with an ellipse varies considerably from frame to frame due to noise in the sky background. Although the skies in Chile are quite dark, Virgo can only be observed through an air mass greater than 1.3. Of course, the same air mass problem affects photometry from the UK Schmidt which is at about the same latitude. Our CCD data clearly show an increase in sky noise with air mass.

The parameters that we derive from the surface photometry are listed in Table 3. Column (1) gives the galaxy identification, and column (2) gives the filter through which the deepest image was obtained. Columns (3) and (4) list the extrapolated central surface brightness and scale length of the exponential fit, while column (5) gives the actual measured central surface brightness and its error. The total B magnitude integrated out to the 27 magnitude isophote is in column (6). Column (7) lists the isophotal diameter measured at the $\mu_B = 27.0$ level, while column (8) gives the average surface brightness within this diameter (determined from photometry through elliptical apertures). Columns (9) and (10) give the measured $B-V$ and $V-I$ colors.

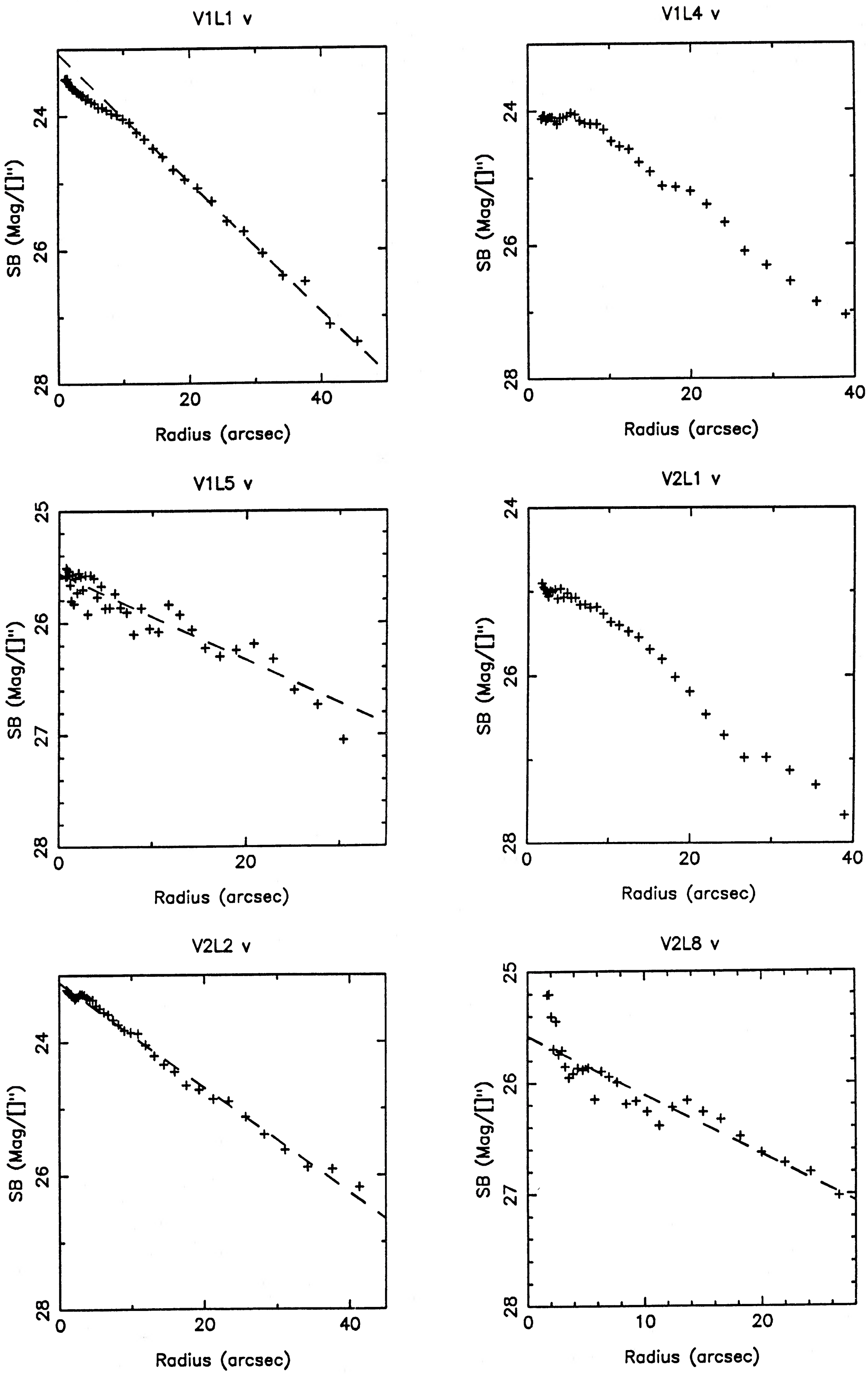

FIG. 2a

FIG. 2.—Azimuthally averaged radial profiles for 26 low surface brightness Virgo dwarfs. Log intensity is plotted against radius, so that an exponential fit is a straight line.

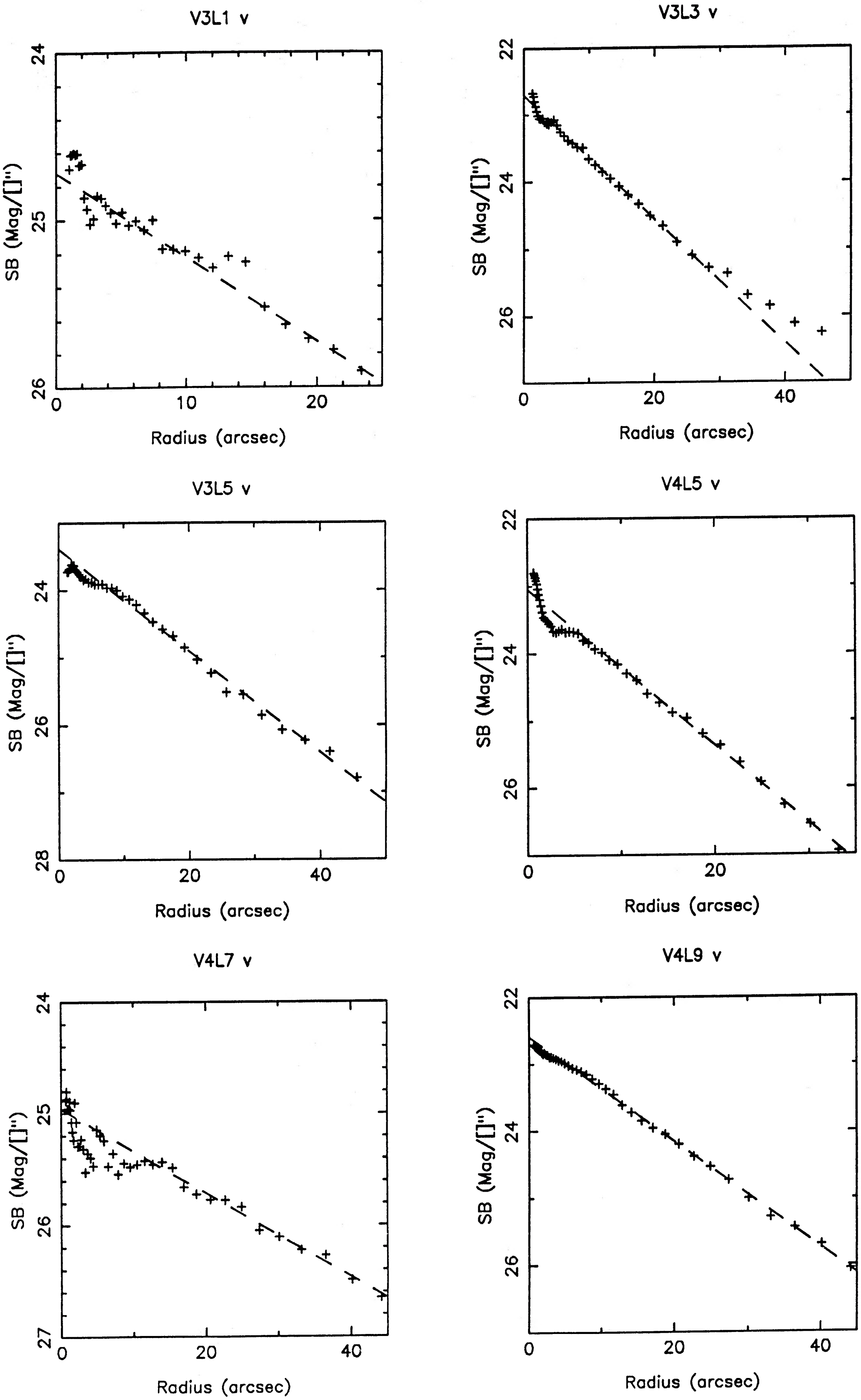
V3L1 v
V3L3 v
V3L5 v
V4L5 v
V4L7 v
V4L9 v
SB (Mag/[]")
Radius (arcsec)
24
25
26
22
28
27
0
10
20
40

FIG. 2b

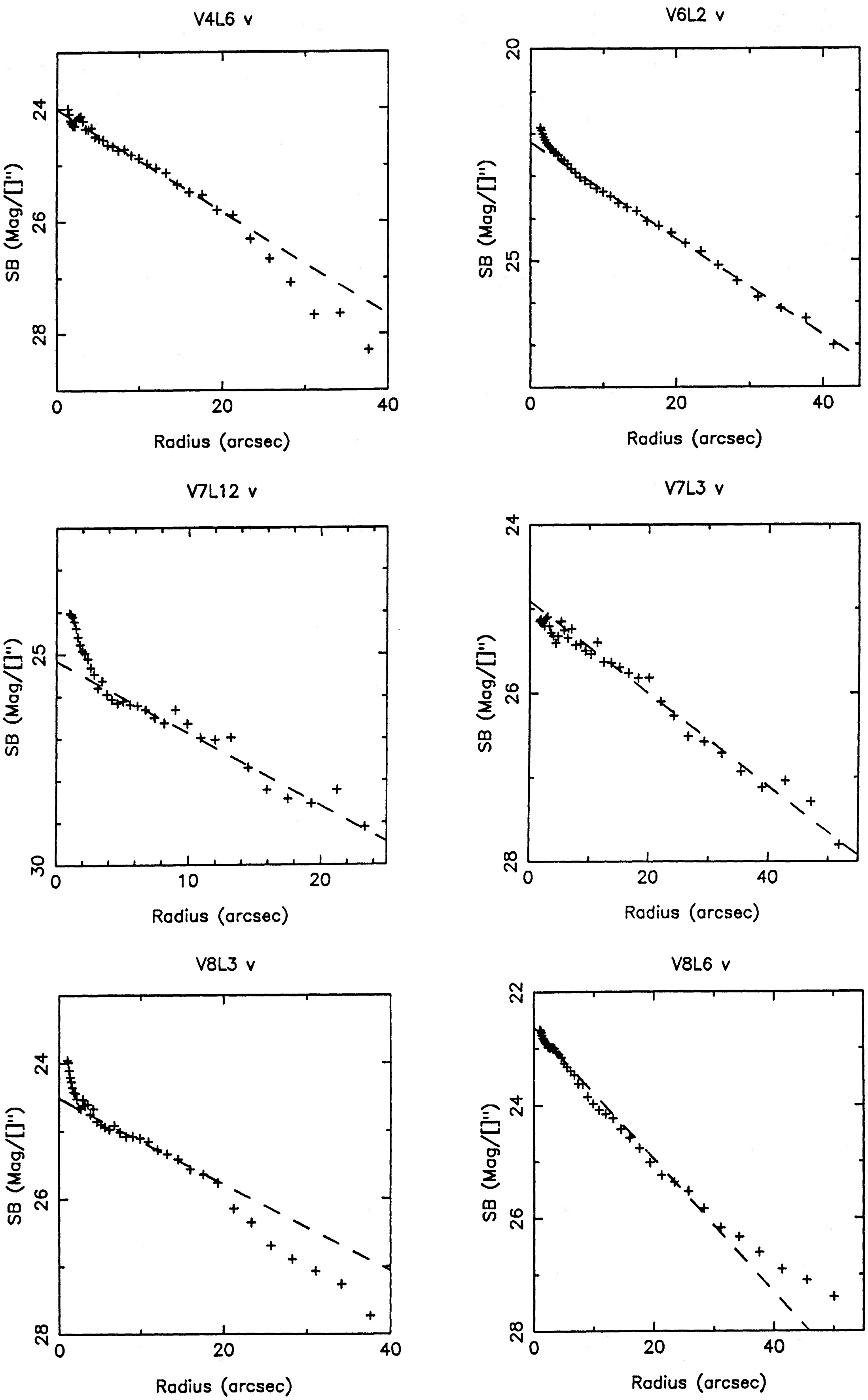
V4L6 v
SB (Mag/[]")
24
26
28
0
20
40
Radius (arcsec)
V6L2 v
SB (Mag/[]")
20
25
0
20
40
Radius (arcsec)
V7L12 v
SB (Mag/[]")
25
30
0
10
20
Radius (arcsec)
V7L3 v
SB (Mag/[]")
24
26
28
0
20
40
Radius (arcsec)
V8L3 v
SB (Mag/[]")
24
26
28
0
20
40
Radius (arcsec)
V8L6 v
SB (Mag/[]")
22
24
26
28
0
20
40
Radius (arcsec)

FIG. 2c

1988ApJ...330..634I

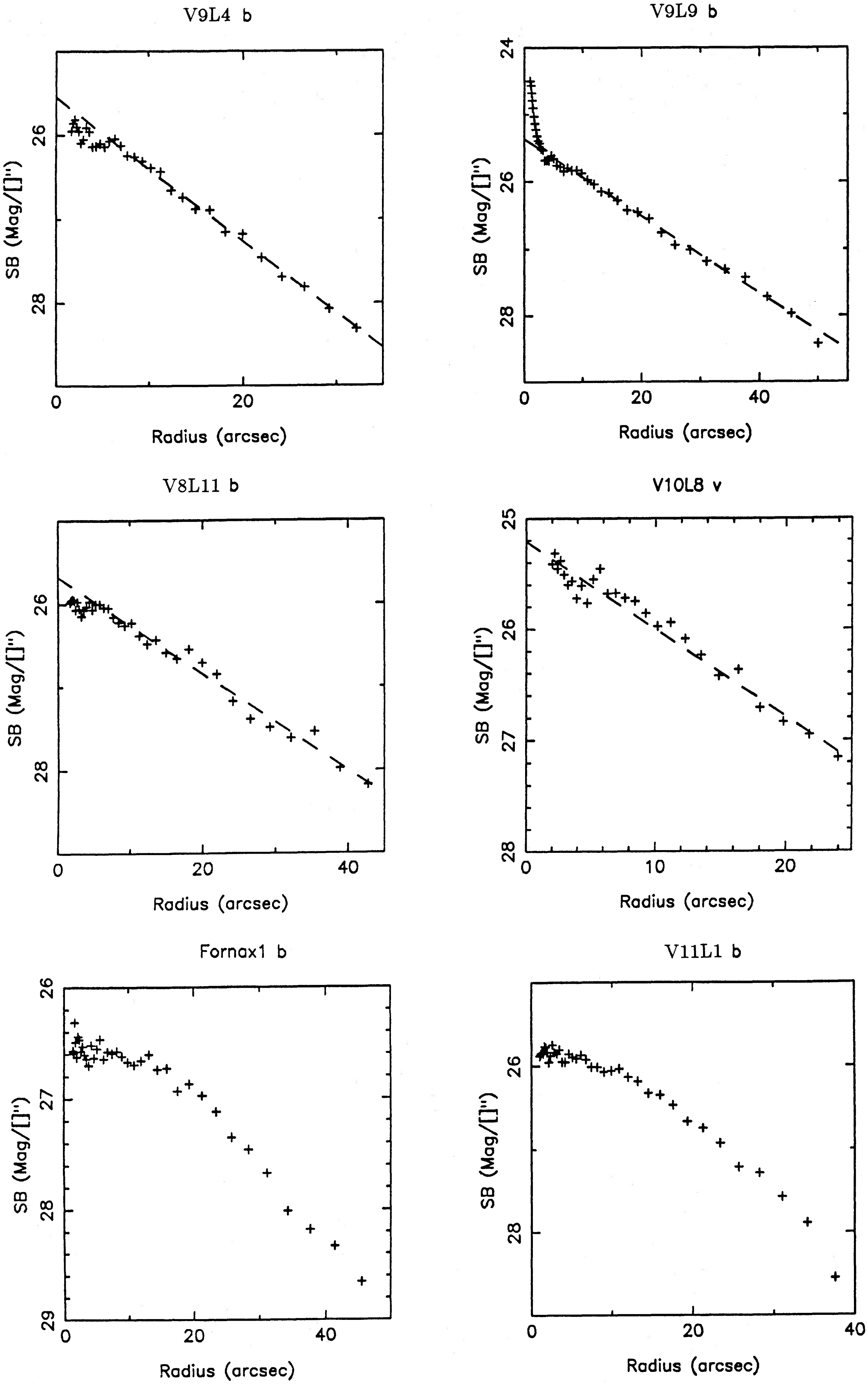

FIG. 2*d*

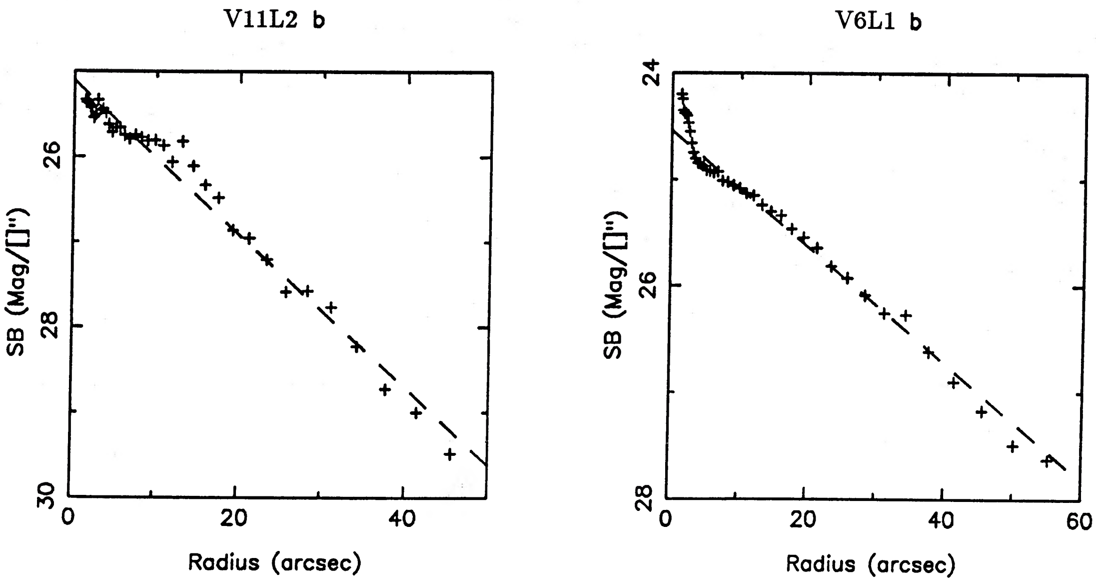

FIG. 2e

TABLE 3

PHOTOMETRY AND STRUCTURAL PARAMETERS

Galaxy	Filter	μ_o	α (arcsec)	$[\mu_o \pm \sigma(\mu_o)]_{meas}$		B_{27}	D_{27} (arcsec)	μ_{27}	B−V	V−I
(1)	(2)	(3)	(4)	(5)		(6)	(7)	(8)	(9)	(10)
V1L1	V	23.64	11.3	24.02	.03	16.6	75	25.05	0.57	0.94
V1L3	V	26.21	45.0	20.45	.03	16.2	120	...	0.95	...
V1L4	V	...	...	24.44	.03	16.6	64	25.16	0.37	0.70
V1L5	V	26.06	28.2	26.00	.10	18.4	46	26.04	...	...
V2L1	V	...	...	25.47	.04	17.7	44	25.60	0.57	0.95
V2L2	V	23.64	13.8	23.75	.03	16.2	86	24.95	0.53	0.93
V2L8	V	25.88	20.5	25.54	.06	18.9	45	26.02	0.30	1.30
V3L1	V	25.22	21.6	25.20	.05	...	...	...	...	...
V3L3	V	23.21	11.7	23.18	.03	15.5	92	24.98	...	...
V3L5	V	24.02	14.4	24.35	.03	16.5	86	25.17	0.63	0.74
V3L8	V	...	...	25.85	.11	...	...	...	...	...
V4L5	V	23.51	9.4	23.26	.03	16.6	55	24.74	0.46	0.83
V4L6	V	24.63	11.9	24.62	.03	17.6	48	25.29	0.62	0.98
V4L7	V	25.46	28.9	25.35	.06	16.8	80	25.77	...	...
V4L9	V	23.25	13.8	23.36	.03	15.6	90	24.70	0.66	0.89
V6L1	B	24.54	19.8	24.20	.06	16.7	84	25.85	0.56	1.10
V6L2	V	22.85	9.5	22.50	.03	15.4	75	24.50	0.65	0.97
V6L6	V	...	...	25.89	.10	...	...	...	...	...
V7L3	V	25.43	19.8	25.67	.06	17.7	53	25.86	0.52	0.90
V7L12	V	25.72	6.3	24.59	.03	20.2	15	25.71	0.56	1.05
V8L3	V	24.86	17.0	24.30	.03	17.4	49	25.56	0.35	0.99
V8L6	V	23.10	9.2	23.15	.03	16.4	71	24.94	0.48	1.08
V8L11	B	25.68	18.7	25.95	.05	18.7	45	26.10	0.52	1.12
V9L4	B	25.55	12.7	25.90	.05	19.0	34	26.15	...	...
V9L5	B	...	...	26.45	.14	...	...	...	...	...
V9L9	B	25.36	18.9	24.50	.03	18.0	56	26.30	0.54	1.21
V10L8	V	25.76	13.7	25.90	.06	18.7	34	25.98	0.55	...
V11L1	B	...	...	25.88	.05	18.5	47	26.29	...	...
V11L2	B	25.11	12.1	25.33	.04	18.7	43	26.19	0.88	0.92
For1	B	...	...	26.57	.08	19.3	43	26.54	0.54	...

For two of the fainter objects, $V-I$ could not be measured even though $B-V$ could. This is a consequence of the very bright sky through the I filter relative to the B filter. These colors are only tabulated when the errors are less than 0.05 and 0.1 mag, respectively. They were typically measured through an aperture of diameter 20" since that yielded the highest S/N colors. Any embedded blobs were masked out in the color determination. In general, these galaxies do not exhibit color gradients. However, there are two galaxies, V2L8 and V6L1, which exhibit quite red nuclei. The colors measured through a 5" aperture are $B-V=0.60$, 0.77 and $V-I=1.89$, 1.86, respectively. These $V-I$ colors are as red as those of luminous ellipticals even though the absolute magnitudes are only $M_B=-10.1$ and -9.1. Possibly, these low-luminosity nuclei could be very metal-rich (Bothun and Mould 1988). This speculation needs spectroscopic confirmation.

b) H I *Observations*

The Arecibo 305 m reflector was used for 21 cm observations of 32 of the low surface brightness galaxies in 1985 October, following the procedure described in Bothun *et al.* (1985). Five minute on-off pairs were used for 29 LSB galaxies, the 1024 channel correlator was set to cover the velocity range -500 to 2500 km s^{-1}. The only detection was Malin 1 (V1L3), with over 10^{11} $M_\odot$ of H I at a redshift of 25,000 km s^{-1}. Malin 1 was also the only galaxy where the receiver was tuned to a large velocity, to match the optically determined redshift of the nucleus. The implications of this completely null result are unclear. Bothun *et al.* (1985) also failed to detect any dE's in the Virgo Cluster. Most of our objects are dE's (according to the classification system of Binggeli *et al.*), so it may be that these LSB galaxies have simply lost all of their gas (see Dekel and Silk 1986). The upper limits on H I content are only 3–5 $\times$ 10^6 $M_\odot$, which correspond to 1% of the mass of these galaxies assuming $M/L_B=10$. Ideally, we would need an upper limit a factor of 10 less than this to be sure that these galaxies are completely devoid of gas. By comparison, the dI's detected by Bothun *et al.* (1985) and Hoffman *et al.* (1987) typically have H I fractional contents of 10%–50%. These new dE's are quite H I–deficient compared with dI galaxies of similar surface brightness and scale length (Bothun *et al.* 1986). The large disparity in H I content once again rules out the possibility that our collection of very LSB dwarfs are merely hibernating gas-rich dwarfs awaiting their next burst of star formation (Tyson and Scalo 1988). Finally, we remind the reader that it is always possible that some of the nondetections are background, intrinsically large objects like Malin 1.

IV. STELLAR POPULATIONS AND AGES

Only one issue will be addressed here as this topic has been discussed in greater detail by Caldwell and Bothun (1987). In general, these very LSB galaxies are blue. The mean colors are $B-V=0.54\pm0.12$ and $V-I=0.98\pm0.15$. Perhaps the best source of comparison is with the most metal-poor Galactic globular clusters. From the compilations of Hesser and Shawl (1985) and Hanes and Brodie (1986), we deduce that the metal-poor Galactic globulars ([Fe/H] <-1.7) have mean $B-V$ and $V-I$ colors of 0.62 ± 0.02 and 0.93 ± 0.05, respectively. The colors of the LSB dwarfs are therefore bluer in $B-V$ but similar in $V-I$ to the most metal-poor Galactic globulars. If this indicates giant branch metallicity, then these galaxies violate the mass-metallicity relation, because, although they would have abundances similar to Draco and Ursa Minor ([Fe/H] ≈ -2), they are 100 times as luminous (because their scale lengths are so large). Alternatively, a reduced mean age with respect to Galactic globulars would also account for their blue colors, especially in $B-V$.

These colors are also signficantly bluer than the colors of Fornax dE's found by Caldwell and Bothun (1987). This is disturbing if low surface brightness is due to faded stellar populations, because the fading must then occur in a manner that does not cause the stellar population to become redder. Since the fading of stellar populations is due to the disappearance of upper main-sequence stars as they begin to populate the giant branch, some very simple considerations would be violated. Hence, it is difficult to understand the blueness of these low surface brightness galaxies. We can at least state that they are unlikely to bias or contaminate faint galaxy counts aimed at determining galaxy evolution (e.g., Koo 1986). In other words, LSB dwarfs such as these cannot mimic the properties of LSB galaxies at high redshift [made LSB by $(1+z)^4$ dimming] because they simply are not red enough.

Our overall conclusion regarding stellar populations and ages is that these very LSB galaxies must be composed of metal-poor, yet moderately young, stars. The $B-V$ colors especially are too blue for an old stellar population. A composite metal-poor giant branch plus a substantial F main-sequence star population can account for the observed colors. But we must emphasize what appears to be a paradox. We have discovered a class of galaxies with surface brightness (and hence surface mass densities) that can be up to 100 times less than those found in more normal galaxies. Yet the inferred stellar population is similar to conventional stellar populations. This is an enigmatic result—what star formation history/process can produce a more or less normal stellar population in which the average separation between stars (i.e., surface brightness) is so low? Put another way, a central surface brightness of $(\mu_0)_B=25.0$ corresponds to a surface density of luminous matter of 5 $L_\odot$ pc^{-2} (assuming solar neighborhood IMF). If the M/L is normal, then the implied surface mass density is also very low. Such low surface mass densities are conducive to the overall expansion of these systems, a possibility that cannot be ruled out on the basis of our data.

V. STRUCTURAL PARAMETERS AND SELECTION EFFECTS

In this section we attempt to understand the selection effects on the observed distribution of galaxy structural parameters. Despite their convenience, isophotal magnitudes and diameters may not be the most useful tools available. A comparison will be made between the structural parameters of this sample of low surface brightness galaxies and previous observations of low-luminosity galaxies. The previous work in Virgo is by Caldwell (1983, hereafter C), Binggeli, Sandage, and Tarenghi (1984, hereafter BST84), and Ichikawa, Wakamatsu, and Okamura (1986, hereafter IWO). Dwarf galaxies in the Fornax cluster are taken from Caldwell and Bothun (1987, hereafter CB). Finally, we include in the comparison the dwarf spheroidals in the Local Group, as discussed by Faber and Lin (1983). Parameters for Fornax and Local Group galaxies are adjusted to the distance of Virgo assuming d(Virgo) = 1.25 d(Fornax), the distances given in Faber and Lin, and a Virgo distance modulus of $m-M=31.7$. All photometric properties will be given in the B band, unless otherwise stated. We have assumed $B-V=0.5$ to derive numbers for our new galaxies where the radial profile was measured in the V band. These combined data sets do not in any way constitute a complete sample. It is perhaps questionable to include Malin 1 in these comparisons since it is such an extraordinary object. The enormous gas-rich disk in Malin 1 is very different from the small gas-free spheroids of most dwarf ellipticals. Yet it would be wrong to exclude it *a posteriori*, since the spiral features were not visible on the discovery photograph, and only showed up on the subsequent CCD frame. Its inclusion is a reminder of our ignorance of the redshift and nature of *most* low surface brightness galaxies.

a) Exponential Radial Profile

The validity of an exponential fit to the radial profile of low luminosity galaxies has been confirmed by many workers (BST84; IWO; CB). The two parameters of the exponential fit are the scale length (α) and the extrapolated central surface brightness (μ_0). Simple relationships between characteristics of an exponential profile are summarized for convenience in the Appendix. We prefer central surface brightness and exponential scale length to the more commonly used effective surface brightness and effective radius for the following reason. The latter parameters require a knowledge of the total magnitude integrated out to a large radius. The total magnitude of a faint galaxy is necessarily uncertain, because it is very sensitive to the correct setting of the sky level and the dynamic range of the detector. On the other hand, the determination of α and μ_0 uses only the information in the highest signal-to-noise ratio parts of the image. Total magnitudes are obtained by integrating α and μ_0 to infinity. Therefore, *if* the exponential is a good model of the radial profile, then α and μ_0 are optimal for describing faint galaxies.

It is known that somewhere around $M_B \approx -16$ marks a transition between profiles fitted purely by an exponential and galaxies with an $r^{1/4}$ component in the central regions (CB). Also, the luminosity range over which galaxies are fitted by exponential profiles is much larger than the luminosity range fit by $r^{1/4}$ profiles. Figure 3*a* shows the fraction of galaxies with an $r^{1/4}$ component as a function of total B magnitude using the combined data set described above. Below $B_{\rm tot} = 17$, the fraction of galaxies with an $r^{1/4}$ component drops rapidly to under 15%. Figure 3*b* shows the fraction of galaxies with stellar nuclei dropping with magnitude, as originally demonstrated by BST84. The fraction of nuclei is higher at a given magnitude than found by BST84, probably due to the fact that for galaxies with radial profiles, nuclei can be recognized down to the level of 0.1% of the total magnitude. The distinction between $r^{1/4}$ components and nuclei is difficult to make, since some of the nuclei we observe could be spatially unresolved $r^{1/4}$ components. However, in almost every case, the *dominant* component (90% or more of the integrated light) has an exponential profile.

Figure 3 indicates the diminishing importance of non-exponential components for the faintest galaxies. How good is the exponential fit? In the two studies that used linear CCD detectors (this work and CB), the data covers two to three scale lengths with no signs of substantial deviations. To test the exponential model at low light levels, we fitted the profile between $\mu = 25$ and 26 mag arcsec^{-2} and extrapolate to $\mu = 27$ mag arcsec^{-2}. For each galaxy, the difference between the actual and extrapolated surface brightness $\Delta\mu = \mu_{27} - \mu_{27}{}^*$ can be measured. The CCD data for 52 galaxies gives $\Delta\mu = 0.03 \pm 0.20$, an undetectable deviation from an exponential fit. The photographic data, however, show systematic deviations to a slope steeper than an exponential at the faintest levels. The values of $\Delta\mu$ are 0.18 ± 0.28 (C), 0.68 ± 0.36 (BST84), and 0.32 ± 0.11 (IWO). We believe that this steepening is due to either a calibration problem or a difficulty in selecting the appropriate sky level in the photographic samples. Photographically, the level of $\mu = 27$ is often the faintest isophote measured and is very sensitive to placement of the sky level. Also, there are acknowledged problems in the conversion of density to intensity. The CCD data is linear to better than 1%, with a superior dynamic range. The uniformity of the flat field means that in some cases the profile can be followed out to 29 or 30 mag arcsec^{-2}, or a factor of 10 fainter than typical photographic material. Apart from the caution that should be attached to the faintest photographic isophotes, the radial profiles of most galaxies of $M_B > -16$ are exponential.

b) Total Magnitudes

A total magnitude can be determined either from the integration under the radial profile or by calculation from the parameters of the exponential fit. For a comparison between the two, the nuclear light must be subtracted from the asymptotic magnitude, since the extrapolated central brightness of the exponential fit takes no account of the nucleus. For the CCD samples, the difference between the two is small, $\Delta B = B_{\rm tot}(\text{asymptotic}) - B_{\rm tot}(\text{exponential}) = 0.05 \pm 0.20$. However, there is a systematic shift in ΔB for the photographic samples, values of ΔB are 0.12 ± 0.21 (C), 0.33 ± 0.29 (BST84), and 0.20 ± 0.15 (IWO). The sense of the shift is that photographic asymptotic magnitudes are fainter than total magnitudes from an exponential fit, and the cause once again is the depression of the lowest photographic isophotes. Figure 4 shows the distribution of ΔB, and there is no strong dependence on magnitude for any of the samples. We can confirm this magnitude offset for the galaxies with CCD photometry in this paper, because most of them have total magnitudes from BST84. The mean difference is $B_{\rm tot}(\text{BST84}) - B_{\rm tot}(\text{this work}) = 0.37 \pm 0.50$, excluding the five galaxies with photographic magnitudes flagged as being of poor quality. Therefore, we find that published photographic total magnitudes tend to underestimate the total flux in faint galaxies by about 30% (with large scatter). Having demonstrated the applicability of exponential fits, in future we use total magnitudes calculated using μ_0 and α.

c) Central Surface Brightness

Three diagrams will be used to study the structural parameters of low surface brightness galaxies. Figure 5*a* shows central surface brightness plotted against total B magnitude or, equivalently, luminosity, with prevous galaxy samples shown as crosses (galaxies from C, BST84, IWO, and CB) and open circles (Local Group DSs). The new measurements are the filled circles. With its magnitude adjusted to the distance of the Virgo cluster, Malin 1 lies far removed from bulk of the galaxies. Clearly it is an extraordinary galaxy. Yet the rest of the low surface brightness galaxies also have little overlap with previous measurements. In particular, at a low value of central surface brightness, the well-known relationship between central surface brightness and luminosity breaks down completely. From $M_B = -16$ to -14 (or $B_{\rm tot} = 15.7$–17.7), the spread in central surface brightness at a given luminosity doubles. The striking feature is that despite their central surface brightnesses of only a few per cent of the night sky, this

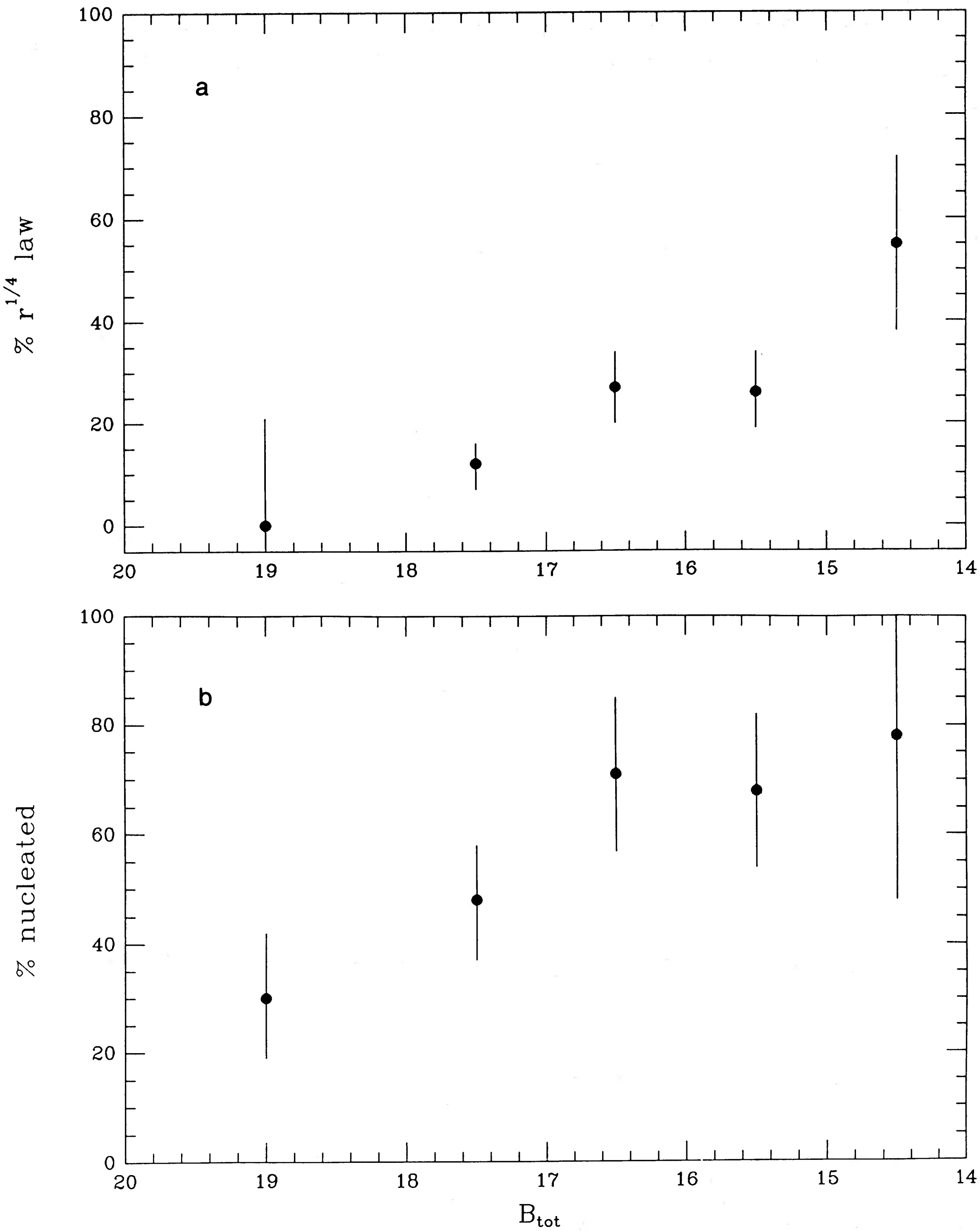

FIG. 3.—(*a*) The fraction of galaxies having central regions fit by an $r^{1/4}$ power law as a function of total *B* magnitude, from the combined dwarf samples discussed in the text. (*b*) The fraction of nucleated dwarfs as a function of total *B* magnitude, where the detection limit on nuclei is 0.1% of B_{tot}.

study has not isolated particularly low luminosity galaxies. Figure 5*b* shows the same plot on a scale that excludes Malin 1, with tracks overlaid that indicate the selection effects involved. The solid diagonal lines are tracks of constant exponential scale length, and the dashed lines are tracks of angular size at a limiting surface brightness μ_{lim}. The expression for θ_{lim} was derived by Allen and Shu (1979) and is repeated for convenience in the Appendix. Five tracks show the limiting angular size for different values of limiting surface brightness. The limiting surface brightness is defined as the level at which the galaxy isophotes disappear into the background on (for example) a photographic plate.

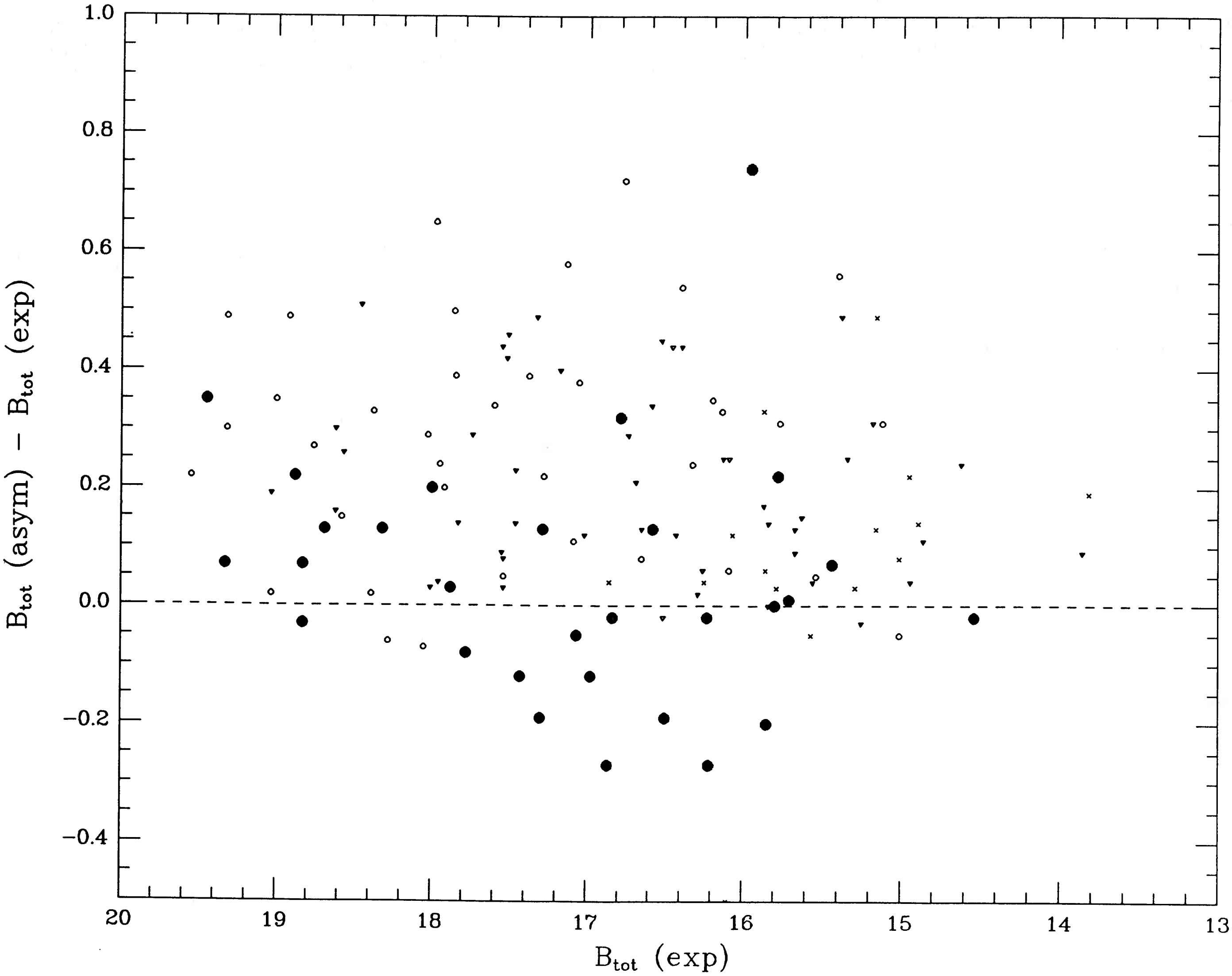

FIG. 4.—The difference between total magnitudes calculated from the asymptote of the light distribution and from the parameters of an exponential fit to the radial profile. The symbols represent this study and CB (*filled circles*), C (*crosses*), IWO (*triangles*), and BST84 (*open circles*).

The explanation for the previously observed relation between central surface brightness and luminosity has been emphasized by Allen and Shu (1979) and Disney (1980). At any given luminosity, galaxies tend to be chosen which give the largest angular size at a limiting isophote. For deeper and deeper surveys and increasing values of μ_{lim}, this maximum angular size occurs for lower and lower central surface brightness. Taking a limiting angular size of 20″ (appropriate for BST85), the sequence of tracks as a function of μ_{lim} follows previous data well. The new data (*filled circles*) are bounded by a track of $\theta_{lim} = 50''$, $\mu_{lim} = 28$ mag arcsec^{-2}. In other words the selection of galaxies of large angular size has naturally led to a large number of objects with μ_0 as faint as 26 mag arcsec^{-2}. A survey designed to detect objects like the Local Group DSs at the distance of the Virgo Cluster would have to search down to $\mu_{lim} = 27$ mag arcsec^{-2} and be sensitive to galaxies with scale lengths of a couple of arc seconds and limiting angular sizes of only 5″. At this point, they would probably be regarded as background galaxies. To summarize, the placement of galaxies on the μ_0 versus B_{tot} plane is bounded at faint μ_0 by the limiting isophote level, at faint B_{tot} by the limiting angular size, and at bright μ_0 and at faint M_{tot} by the problem of resolving stars from galaxies. The only direction that is substantially free of selection effects is toward bright B_{tot}, provided that $\mu_0 < \mu_{lim}$.

d) Isophotal Angular Size

Another commonly used diagram is the plot of angular size at a given isophote versus total magnitude or luminosity. Figure 6*a* shows the data, with the same symbols as before and limiting isophotes at $B = 27$ used. There is a remarkably tight relationship between luminosity and isophotal angular size. In particular, the upper envelope of the relationship is very sharp, with one line extending over 14 mag from Malin 1 to the Local Group DS. Figure 6*b* shows the data replotted on a scale that excludes Malin 1, with tracks similar to those on Figure 5*a*

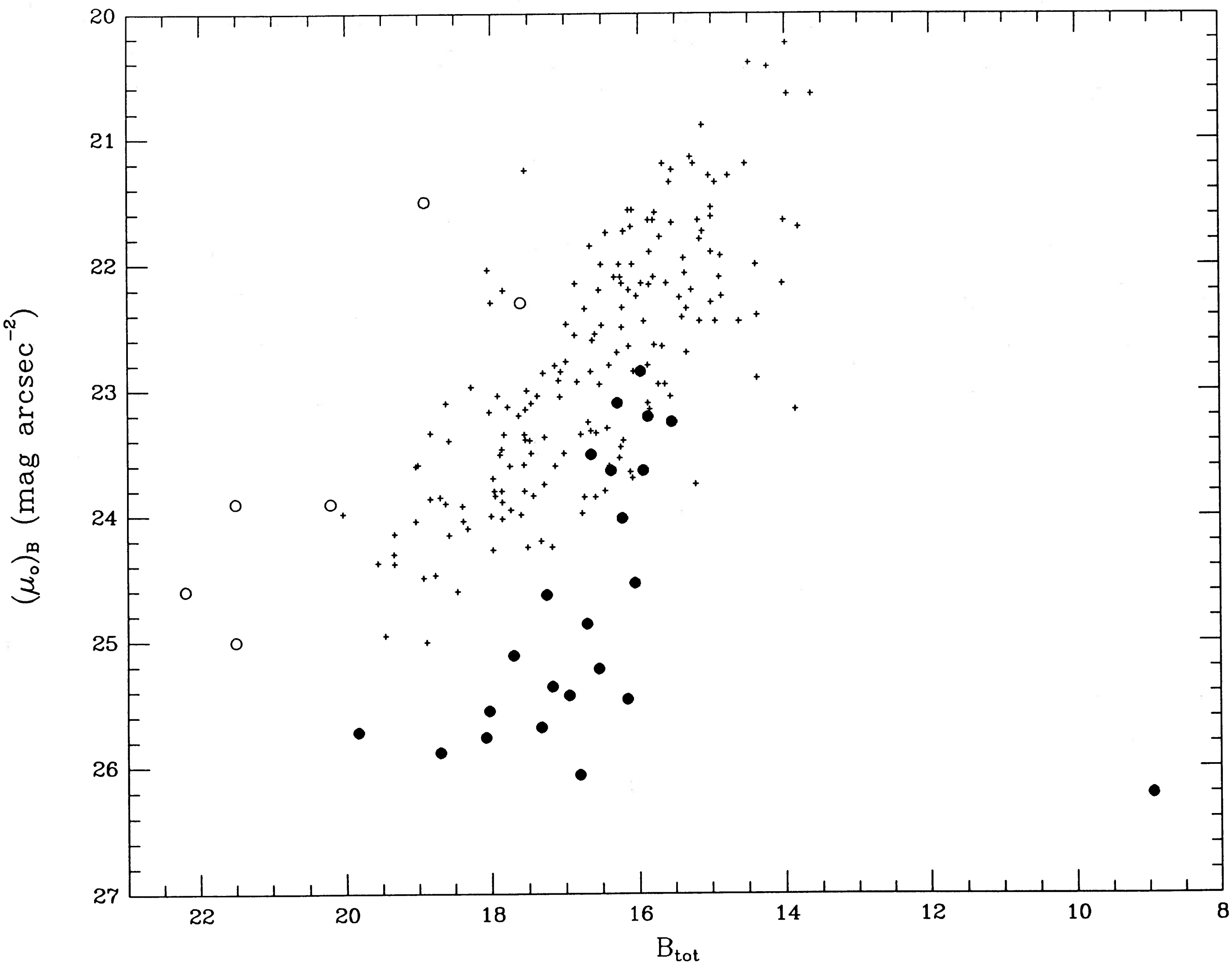

FIG. 5a

FIG. 5.—(a) Central surface brightness vs. total magnitude for previous galaxy samples (*crosses*), this study (*filled circles*), and DS galaxies in the Local Group (*open circles*). Malin 1 lies off to the right. (b) The same plot (excluding Malin 1) with tracks of exponential scale length, and tracks of limiting angular size for a given limiting surface brightness.

added. It now becomes clear that there is actually very little new information added in a plot of D_{27} versus B_{tot}. The sharp upper envelope is a restatement of the fact that for a given luminosity and value of μ_{lim}, galaxies of the largest angular size tend to be selected. The increased depth of the photographically amplified plate material can be seen in the higher boundary line for the new observations. The sharpness of the upper envelope is a confirmation of the accuracy of an exponential model for the radial profiles. However, the tracks of both exponential scale length and central surface brightness are double valued in this diagram. For a specific angular size, there are many combinations of α and μ_0 that correspond to each luminosity.

e) *Exponential Scale Length*

The last plot of interest is that of exponential scale length versus luminosity. Figure 7a shows the distribution, with the enormous and luminous spiral disk of Malin 1 lying off to the side as an anomalous point. This figure also emphasizes that the new galaxies break down the apparent relation between scale length and luminosity. As before, the model tracks are laid down on the data (excluding Malin 1) in Figure 7b. The selection effects already mentioned apply here, and galaxies are never directly selected by scale length (whereas they are directly selected by central surface brightness and isophotal angular size). Nevertheless, a few points can be made. Note that the expected range of luminosity decreases rapidly with increasing scale length. To find large numbers of galaxies with scale lengths greater than 10″ will require searches to smaller limiting diameters, or more effectively, to a fainter limiting surface brightness. Also, the problem of distinguishing stars and galaxies is a strong limitation on discovering galaxies with small scale lengths (i.e., diminished versions of M32 and NGC 4486B). Two horizontal lines on Figure 7b show the position of

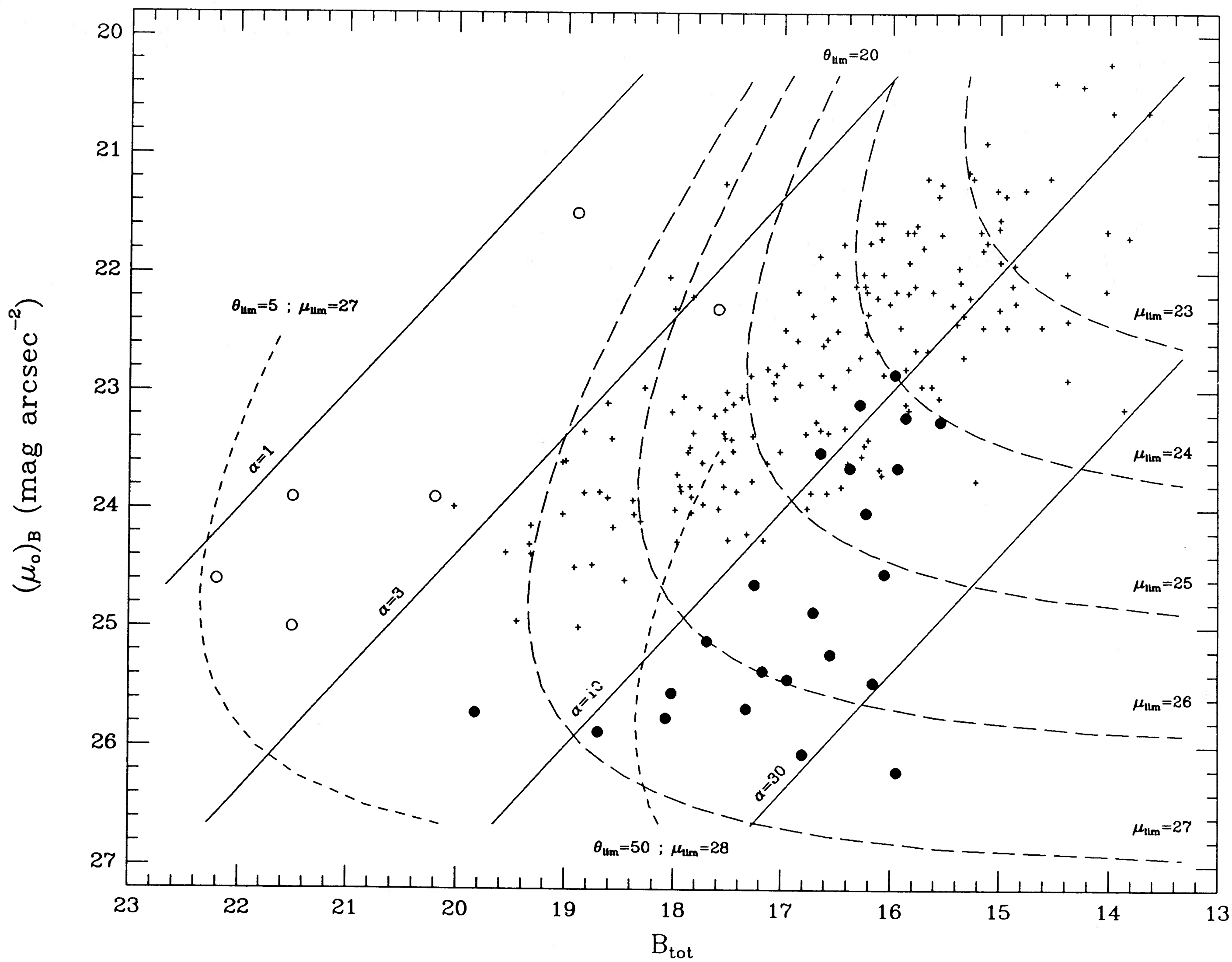

FIG. 5b

Gaussian images of FWHM 1″ and 3″. Between these lines it is difficult to resolve a galaxy on typical wide-field photographs.

f) The Effect of Nuclei

Nuclei are preferentially found in redder and higher luminosity galaxies, the former fact probably indicating higher metallicity in the nucleated galaxies (Caldwell and Bothun 1987). The typical level of nucleation is shown in Figure 8*a*, where nuclear *B* magnitude is plotted against total *B* magnitude for the Virgo and Fornax samples described previously. Only 15% of the nucleated galaxies have more than 10% of the luminosity in the nucleus, and over 50% have less than 3% of the luminosity in the nucleus. Therefore, the nucleus is a small luminosity component in most dwarf galaxies. Figure 8*b* illustrates a quite different situation in terms of surface brightness. Extrapolated central surface brightness from the exponential fit is plotted against the observed central surface brightness (we note that the contrast of an unresolved nucleus is a function of seeing). The upper envelope in this figure means that there are no values of μ_0(exp) − μ_0(meas) greater than 2 in the range $22 < \mu_0 < 24$. In other words, the nuclei show a maximum fractional light contribution. Two selection effects that apply to galaxy samples are evident in this diagram. First, at central surface brightness from 21 to 24 mag arcsec^{-2}, the actual value of μ_0 is on average 1 mag (and up to 2 mag) above the extrapolated value of μ_0. Therefore a luminosity component of only 3% provides a factor of 2 contrast in surface brightness against the night sky. When working near the limit of photographic material, the prominence of a nucleus can make all the difference between selecting a galaxy and passing over what appears only to be a patch of slight density enhancement.

Malin 1 provides a spectacular example of this effect. On the amplified photograph, this galaxy was notable for a large and lumpy envelope and a resolved nucleus. Essentially, it was the prominent bulge component of Malin 1 that drew attention to the enormous submerged disk (and enabled a redshift to be obtained). Even at the distance of Virgo, Malin 1 would be difficult to identify as an impressive galaxy. The bulge com-

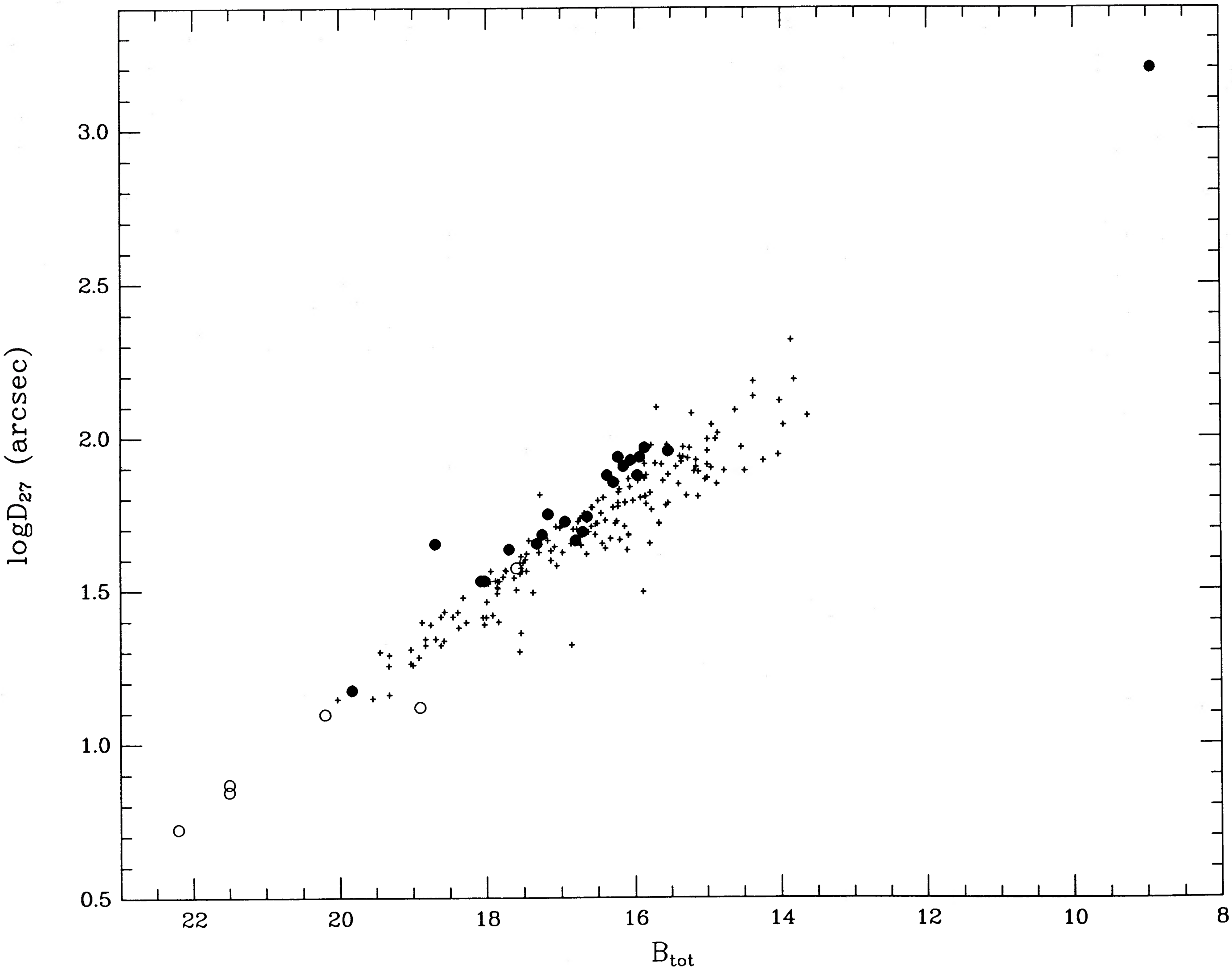

FIG. 6a

FIG. 6.—(*a*) Angular diameter in arcsec at the $\mu_B = 27$ mag arcsec^{-2} isophote vs. total magnitude. Symbols as in Fig. 4. (*b*) The same plot (excluding Malin 1) with tracks of exponential scale length and limiting angular size. Tracks of constant central surface brightness are parallel diagonal lines.

ponent would have the properties of a bright Virgo elliptical, but the low surface brightness disk would cover nearly 30′ at a level of 1% of the sky brightness (cf. Phillipps and Disney 1985). Also, the massive H I disk would overfill the small primary beams of the most sensitive 21 cm telescopes and remain undetected. At the lower central surface brightness levels (and generally lower luminosities), fewer galaxies have nuclei. We also find significant numbers of galaxies with flat cores, where the actual central surface brightness is fainter than the extrapolated value from the exponential fit. The word "core" is used in the sense of a King model with a large core radius. All eight dwarfs with flat cores in the combined galaxy sample have $B_{tot} > 17$. The fraction of galaxies with $B_{tot} > 17$ having flat cores is uncertain but is roughly 10%. These galaxies will be strongly selected against any existing sample, because the flat core diminishes the contrast with the night sky.

Finally, we can test a prediction of Norman, May, and van Albada (1985) that nucleated dEs will be one or two ellipticity classes rounder than nonnucleated dE's. The cause is scattering of radial orbits of the central density cusp. Figure 9 gives the histogram of b/a for all galaxies in our combined sample, for those brighter than $B_{tot} = 17$, and for those with detectable nuclei. There is a slight tendency for nucleated dwarfs to be rounder, but it is not statistically significant.

VI. LUMINOSITY FUNCTION OF DWARF GALAXIES

One of the primary goals of a study of dwarf galaxies is the determination of the luminosity function. Dwarf galaxies are the most common stellar systems in the universe, and their contribution to the integrated mass spectrum of galaxies may be significant. Observational selection has limited the scope of luminosity functions determined from magnitude or volume-

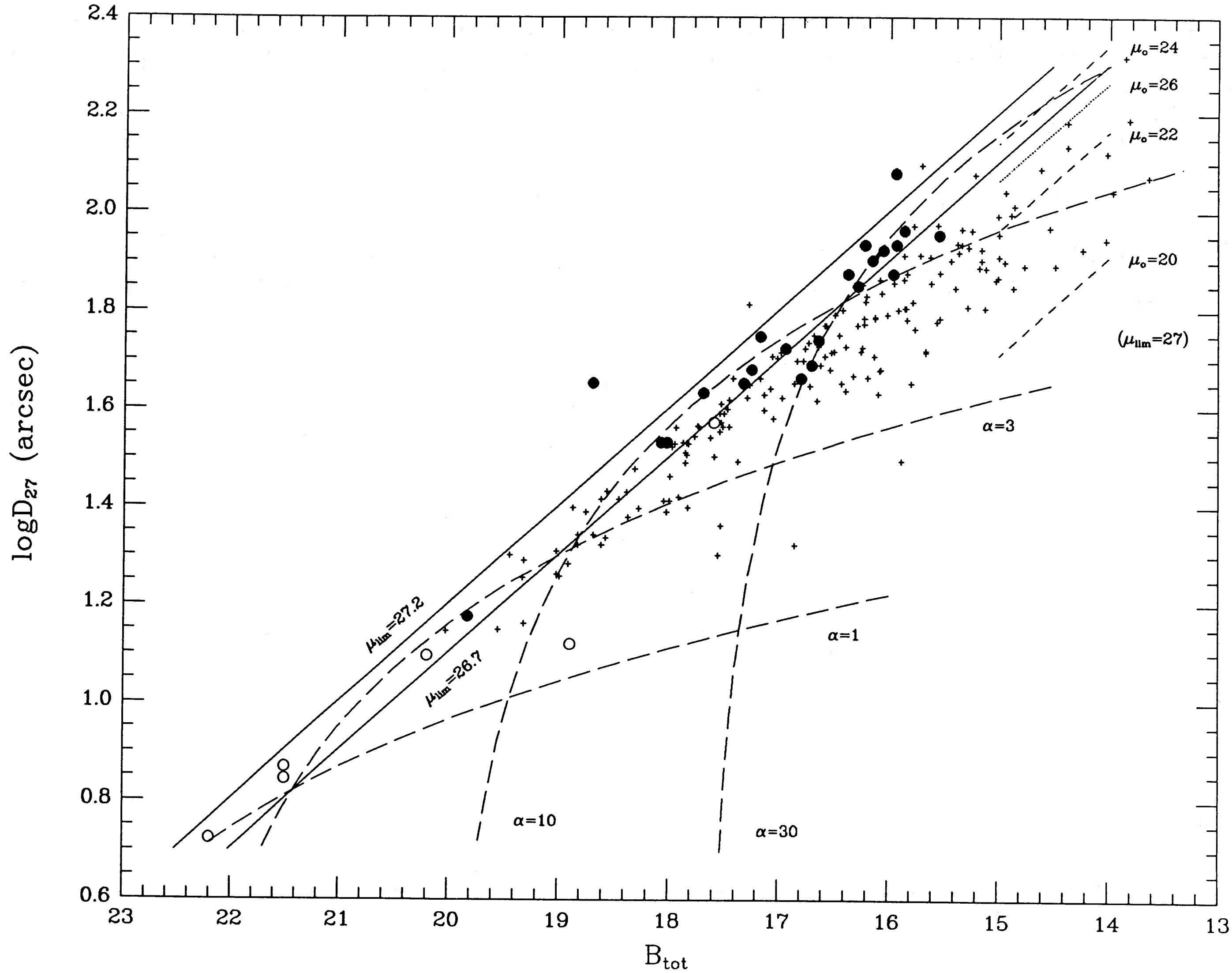

FIG. 6*b*

limited samples. Sandage, Binggeli, and Tammann (1985, hereafter SBT85) have presented luminosity functions for Virgo galaxies down to $M_B \approx -12$, subdivided according to morphological type. We take this impressive work as our starting point.

a) Uncertainties in the Luminosity Function

One of the principal results of SBT85 was that fainter than $B_{tot} \approx 15$, more than half of the galaxies in the Virgo luminosity function are dwarf ellipticals. The fraction continues to increase since there are no dwarf spirals and the dwarf ellipticals have an increasing differential luminosity function. It appears that dwarf ellipticals form a separate family from giant ellipticals, based on the discontinuities in the luminosity function and in core properties (SBT85; Kormendy 1985). Therefore, we restrict our attention to the dwarf elliptical luminosity function of SBT85. The best fit of a Schechter (1976) function to the dE's gives $M^* = 14.3$ and $\alpha = 1.35$, where $\phi(M) = k^{\alpha+1}e^{-k}$ and $k = 10^{0.4(M_* - M)}$. No errors are quoted by SBT85 for the fit. There are critical assumptions, and a sizable correction to apply to the raw luminosity function before this fit is obtained. It is assumed that the BST84 catalog is complete to $B_{tot} \approx 18$ corresponding to an (effective) surface brightness limit of $\mu_{lim} \approx 25.5$ mag arcsec^{-2}. However, it is difficult to derive a total magnitude completeness limit from data which is selected according to surface brightness and angular size, as the last section has illustrated. Half of the galaxies with surface photometry in this paper have $B_{tot} < 18$, and many of them have surface brightness above the limit of previous studies. Their position in Figure 5*b* argues that the completeness limit may be as bright as $B_{tot} = 16.5$–17, because there are a number of galaxies with large scale lengths *and* high luminosities.

A statistical correction for dE's that fall below the detection limit can be applied, as described by SBT85. The method is to extend the upper and lower boundary lines of the relationship between effective surface brightness and luminosity and to calculate the area of the μ_e versus B_{tot} plane that is excluded by observational selection. This leads to a correction factor to the

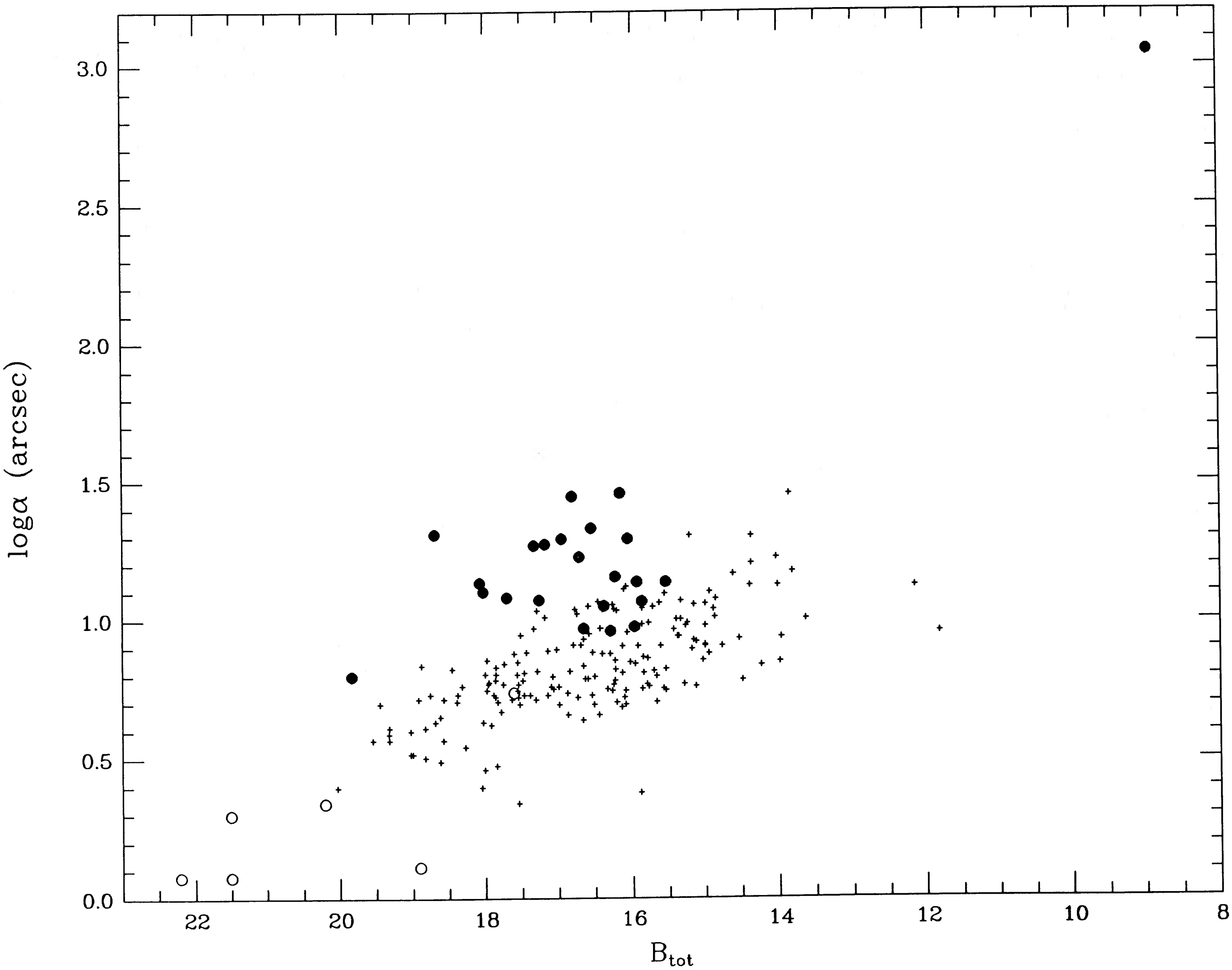

FIG. 7a

FIG. 7.—(*a*) Exponential scale length in arcsec versus total magnitude. Symbols as in Fig. 4. (*b*) The same plot (excluding Malin 1) with tracks of central surface brightness and limiting angular size. The two horizontal dotted lines show exponential scale lengths corresponding to two different FWHM values of a Gaussian point spread function.

counts below the completeness limit and allows the luminosity function to be recovered down to $M_B \approx -12$. We have repeated this calculation, using central rather than effective surface brightness, to see the effect of the new low surface brightness galaxies on the correction. Figure 10 shows several luminosity functions calculated in this way. The lowest curve represents the raw uncorrected counts, and the filled circles represent the corrected function from SBT85. The two lines of crosses give the corrected function using previously published data for two different assumptions of the completeness limit in central surface brightness. The lower curve assumes $\mu_0 = 25$ (including the lowest measured μ_0), and the upper curve assumes $\mu_0 = 24.5$ (the lower envelope in μ_0 of the bulk of the distribution). The curve from SBT85 lies between these two cases. The two lines of open circles give the corrected counts if the galaxies from this study are included. To make the correction a conservative one, we have excluded Malin 1 from the envelope of points. The lower curve assumes $\mu_0 = 26.2$ (nearly the lowest measured μ_0) and the upper curve assumes $\mu_0 = 25.8$ (the lower envelope in μ_0 of the bulk of the distribution).

With the new data, an incompleteness correction must be applied as bright as $B_{tot} = 17$, and the correction is at least a factor of two by $B_{tot} = 18.5$. These large corrections are due to the breakdown of the surface brightness versus luminosity relation for low surface brightness galaxies. The result is a steeper fit to the exponential tail of the Schechter luminosity function. The slope derived for the case where $\mu_{lim} = 25.8$ in the range $15 < B_{tot} < 18.5$ is $\alpha = 1.7$, steeper than the SBT85 value of $\alpha = 1.35$ and not much shallower than $\alpha = 2$, which gives a divergent luminosity spectrum. Figure 1 provides confirmation

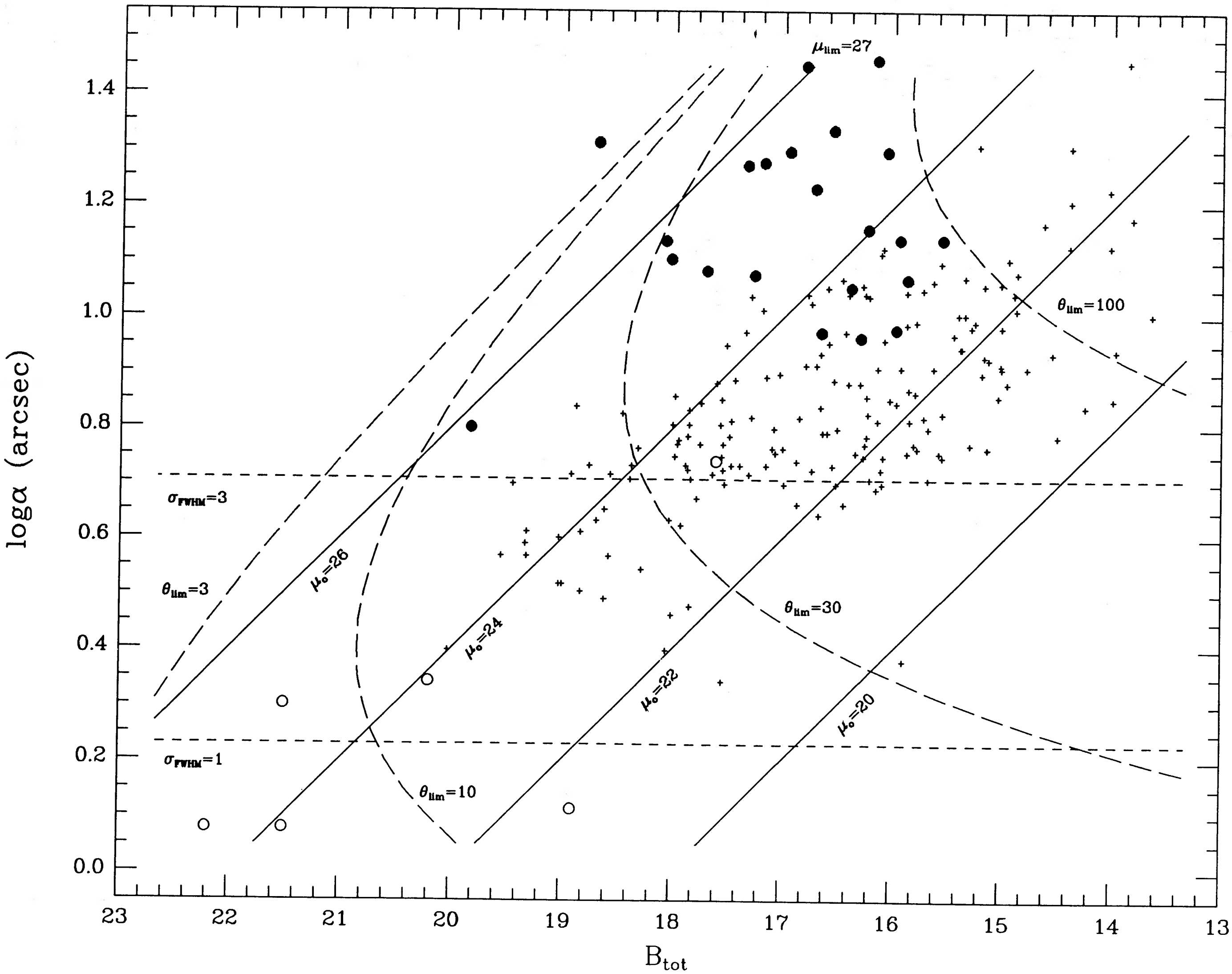

FIG. 7b

that substantial corrections are required to the luminosity function. Although photographic amplification has given a surface density of extreme LSB galaxies that is only 15% of the surface density of previously known galaxies, many of these LSB galaxies are not in the lowest luminosity bin. Figure 1 shows that the newly discovered galaxies (at $\mu \approx 27$) have the same angular size distribution as existing dwarfs (at $\mu \approx 25.5$). Therefore, we suggest that a considerable population remains to be discovered at isophotes fainter than 27 mag arcsec^{-2}.

Our view of the luminosity function of dwarf galaxies is a murky one at best. The calculation carried out by SBT85 is the best that can be done with existing data, but we emphasize the large uncertainties. The completeness correction assumes a uniform distribution of galaxies in the μ_0 versus B_{tot} plane. But our knowledge of the *intrinsic* distribution of galaxy structural parameters is so clouded by observational selection effects that there is no basis for this assumption. The selection against large scale length, low surface brightness galaxies translates into (1) a brighter completeness limit than previously assumed and (2) larger correction factors to the counts. We have discovered that integrated photographic magnitudes for faint dwarfs can be underestimated by 30%–40% due to the difficulty of setting the sky level. All of these factors lead to a steeper slope for the exponential tail of the luminosity function. A final calculation of astrophysical interest is the conversion to a mass function, and the high values of M/L found for Local Group DSs leave open the possibility that the M/L increases with decreasing L (Aaronson and Olszewski 1985). At present, we cannot rule out the possibility that dwarf galaxies represent a significant mass component in the universe.

b) *The Extragalactic Background Light*

Finally, we consider the contribution of extreme LSB galaxies to the extragalactic background light (EBL). In the Virgo Cluster, there is a substantial correction to the luminosity function due to selection effects against low surface brightness and large angular size galaxies. The upper bound to the size of this

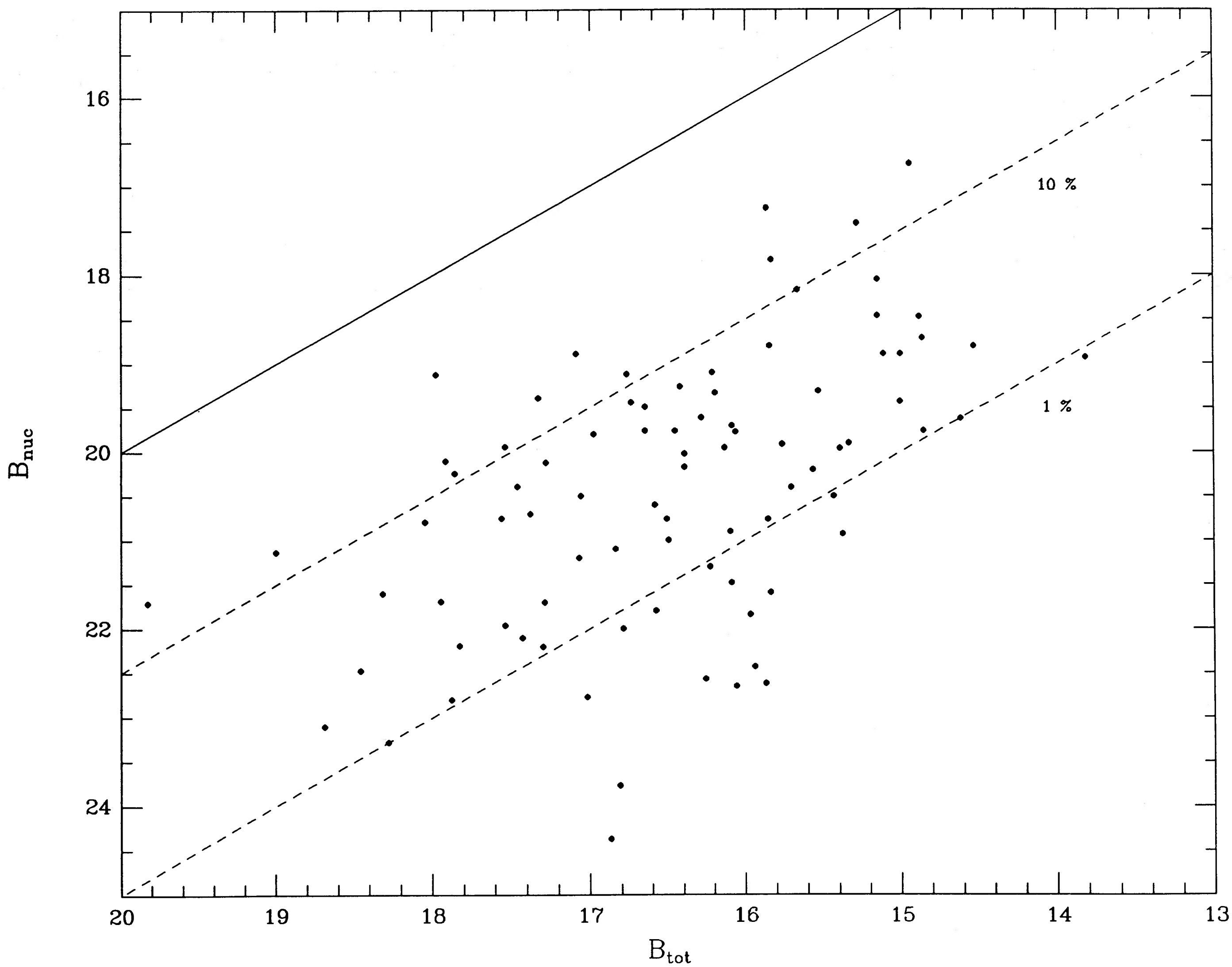

FIG. 8*a*

FIG. 8.—(*a*) Nuclear *B* magnitude plotted against total *B* magnitude for the combined samples discussed in the text. (*b*) Observed central surface brightness plotted against extrapolated central surface brightness from an exponential fit to the radial profile.

correction is related to Olbers's Paradox; the integrated flux from extreme LSB galaxies must not exceed the EBL. In other words, the slope of the luminosity function cannot exceed $\alpha \approx 2$ over a large magnitude range. Dube, Wickes, and Wilkinson (1977) have accounted for zodiacal light and airglow, and quote an upper limit on the surface brightness of the EBL at 5100 Å of $\mu_V < 26.5$. Tyson (1987) has used deep CCD frames to measure low surface brightness objects down to $\mu_B \approx 31$. His measure of the EBL at 4500 Å is obtained by integrating the differential number-magnitude counts of galaxies. The value is $\mu_V = 28.8$ mag arcsec^{-2}.

How does this compare with the light contribution of LSB galaxies in Virgo? The light from the new sample of LSB galaxies in Virgo would contribute $\mu_B \approx 34$ if uniformly spread over the area surveyed. A crude $V/V_{\rm max}$ correction can then be applied since the median angular size of LSB galaxies is 45″, and galaxies as small as 20″ will be detected on the amplified photos. This surface brightness can be integrated out in redshift, correcting for the factor of 3 overdensity of galaxies in Virgo. The surface brightness dimming of $(1 + z)^4$ eventually outweighs the increasing distance, and the integrated surface brightness is dominated by contributions from $z < 0.5$. The total contribution from extreme LSB galaxies is $\mu_V \approx 30.4$, only a factor of 4 fainter than the EBL contribution measured by Tyson (1988). There are substantial assumptions in this calculation. In particular, it is assumed that extreme LSB galaxies follow the spatial distribution of more luminous galaxies and are not confined to clusters. We also note that the contribution to the EBL measured by Tyson is dominated by luminous galaxies with strong UV components due to active star formation. At all magnitude ranges these luminous galaxies have redder $B-I$ colors ($2.0 < B-I < 2.6$) than the extreme LSB galaxies ($B-I \approx 1.5$). Nevertheless, low surface brightness galaxies should not be neglected in any calculation of the EBL.

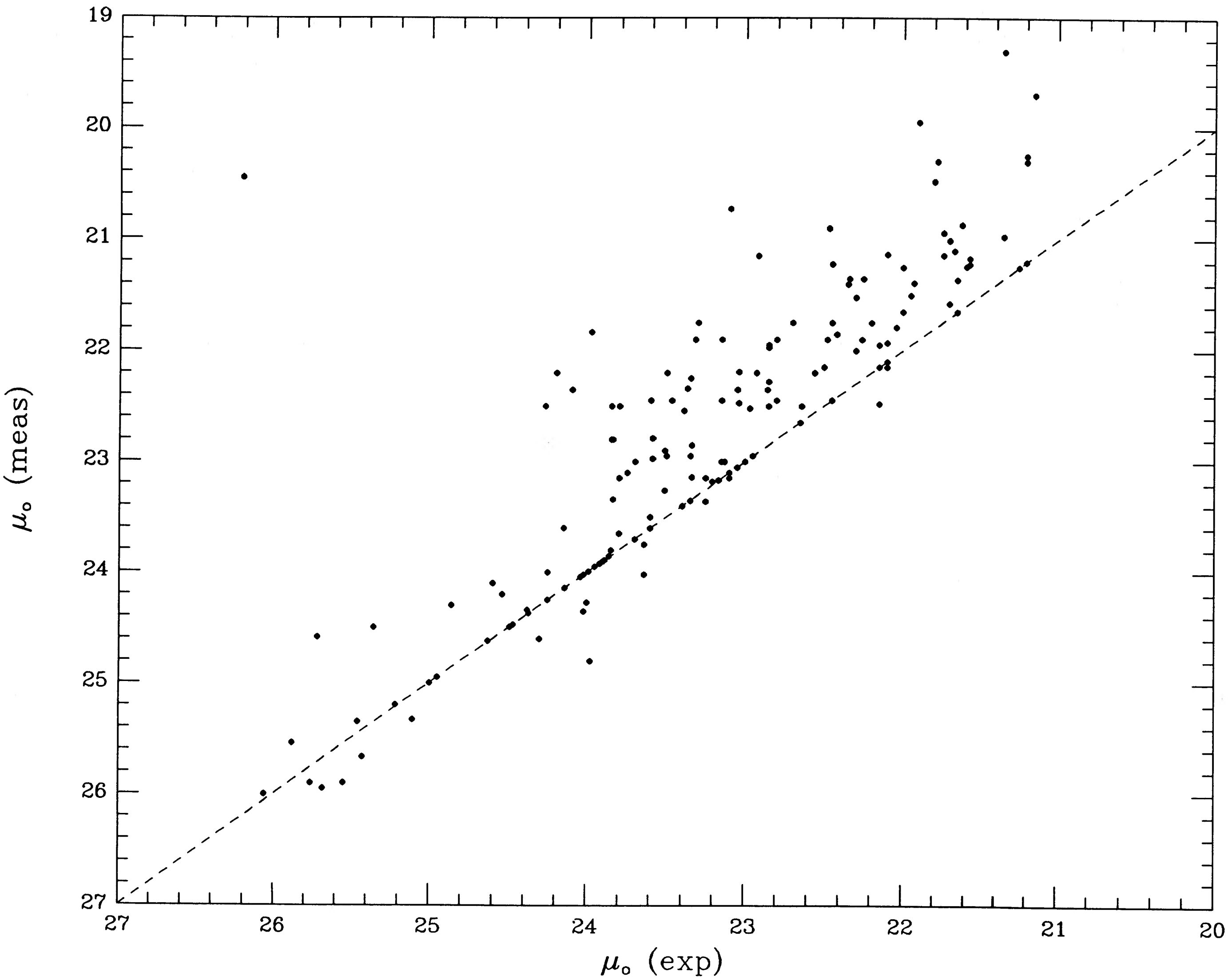

FIG. 8*b*

c) Icebergs in the Sky

In a seminal paper, Disney (1976) proposed that our knowledge of galaxy properties may be seriously biased by the brightness of the night sky. We have confirmed his basic premise and have begun to unmask the selection effects by pushing to a faint surface brightness limit for initial galaxy selection, and by following up with a linear imaging detector on a dark site. Have we succeeded in finding any of the *icebergs* or *crouching giants* discussed by Disney? Figure 11 shows the fraction of galaxy luminosity above the limiting isophote $\mu_B \approx 27$ (i.e., about 1% of night sky brightness) as a function of the limiting angular size (the fraction is quoted in the Appendix). Tracks of constant exponential scale length are superposed. The area covered by previous dwarf galaxy studies is outlined; most of these galaxies have more than 90% of their luminosity lying above 1% of the sky. The new sample extends down to levels where only 20% of the luminosity projects above the limiting isophote. Even when Malin 1 is included, the extreme low surface brightness galaxies fall short of being icebergs, traditionally defined as being 90% submerged below the limiting isophote. Although the level of the EBL puts a limit on the total light from faint galaxies, there is one further concern. We can envisage a surface mass density of gas in a forming galaxy that is so low that star formation is severely inhibited. Malin 1 is probably an example of this. In analogy to the dark bodies that make up the stellar mass spectrum below 0.08 $M_\odot$, there may be a mass spectrum of galaxies which remain dark due to the low surface mass density of gas. Our survey has shown that galaxies with very low surface mass density are common. Therefore, we cannot yet claim to know the true population of faint galaxies.

VII. CONCLUSIONS

This study of dwarf galaxies leads to the following conclusions:

1. Photographically amplified UK Schmidt plates have

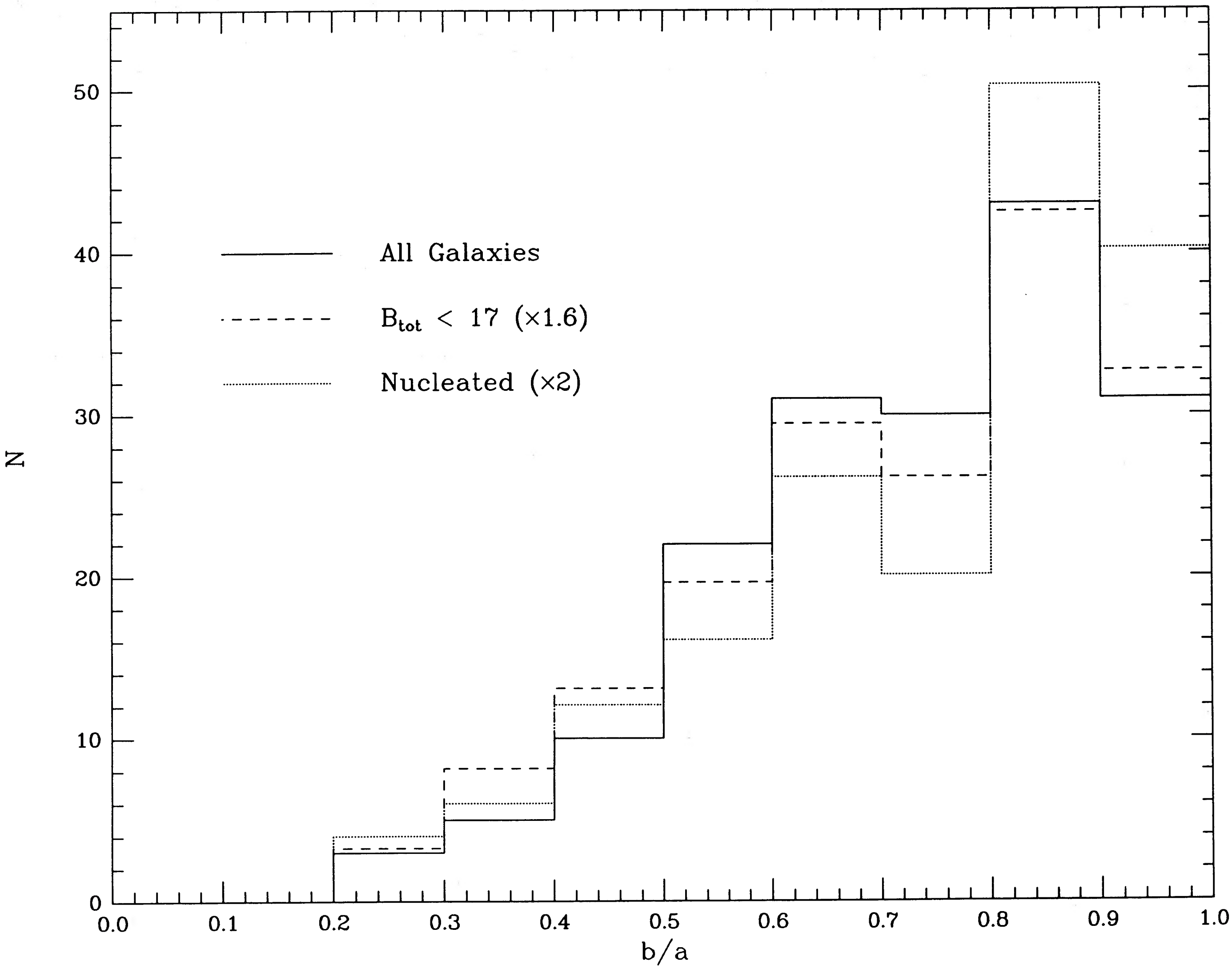

FIG. 9.—Histogram of the distribution of axial ratios b/a for all dwarf galaxies, for the nucleated subset, and for the subset brighter than $B_{tot} = 17$. The differences between the three histograms are not statistically significant.

been used to define a new sample of low surface brightness galaxies in the Virgo Cluster. The limiting isophote for faint galaxy detection is $\mu \approx 27$ mag arcsec^{-2}. Although there is substantial overlap with existing catalogs of Virgo dwarfs, this survey has been successful in finding dwarfs of large angular size and low central surface brightness, which are under-represented in existing catalogs.

2. One of the new low surface brightness galaxies is the largest, most gas-rich spiral galaxy known, located well beyond the Virgo Cluster. The rest appear to be dwarf ellipticals, with upper limits on the amount of neutral material of $M_{\rm H\,I} < 3$–$5 \times 10^6\ M_\odot$. Redshifts are desirable for faint galaxies, because there are unexpected pitfalls in the use of morphology as a distance indicator.

3. CCD photometry shows that the faint galaxies are well modeled by an exponential radial profile, and some of the profiles can be followed down to 29–30 mag arcsec^{-2}, or well below 1% of the night sky brightness. Systematic errors can occur in photographic estimates of total magnitudes for dwarfs; there is no substitute for using a linear detector to measure the properties of low surface brightness galaxies.

4. The colors of very LSB galaxies in Virgo are unusually blue in $B - V$, bluer than the metal-poor Galactic globular clusters. If these galaxies do not violate the mass-metallicity relation then they must have smaller mean ages than Galactic globulars. The star formation history that leads to normal stellar populations with surface luminosity (mass) densities less than 5 $L_\odot$ pc^{-2} is unclear.

5. Our understanding of the intrinsic distribution of dwarf structural parameters is heavily obscured by selection effects imposed by the brightness of the night sky. In particular, the relationship between surface brightness and luminosity breaks down fainter than $M_B \approx -16$. Many of the new dwarfs do not have particularly low luminosity, despite their extremely low surface brightness.

6. We confirm that any faint galaxy survey tends to choose

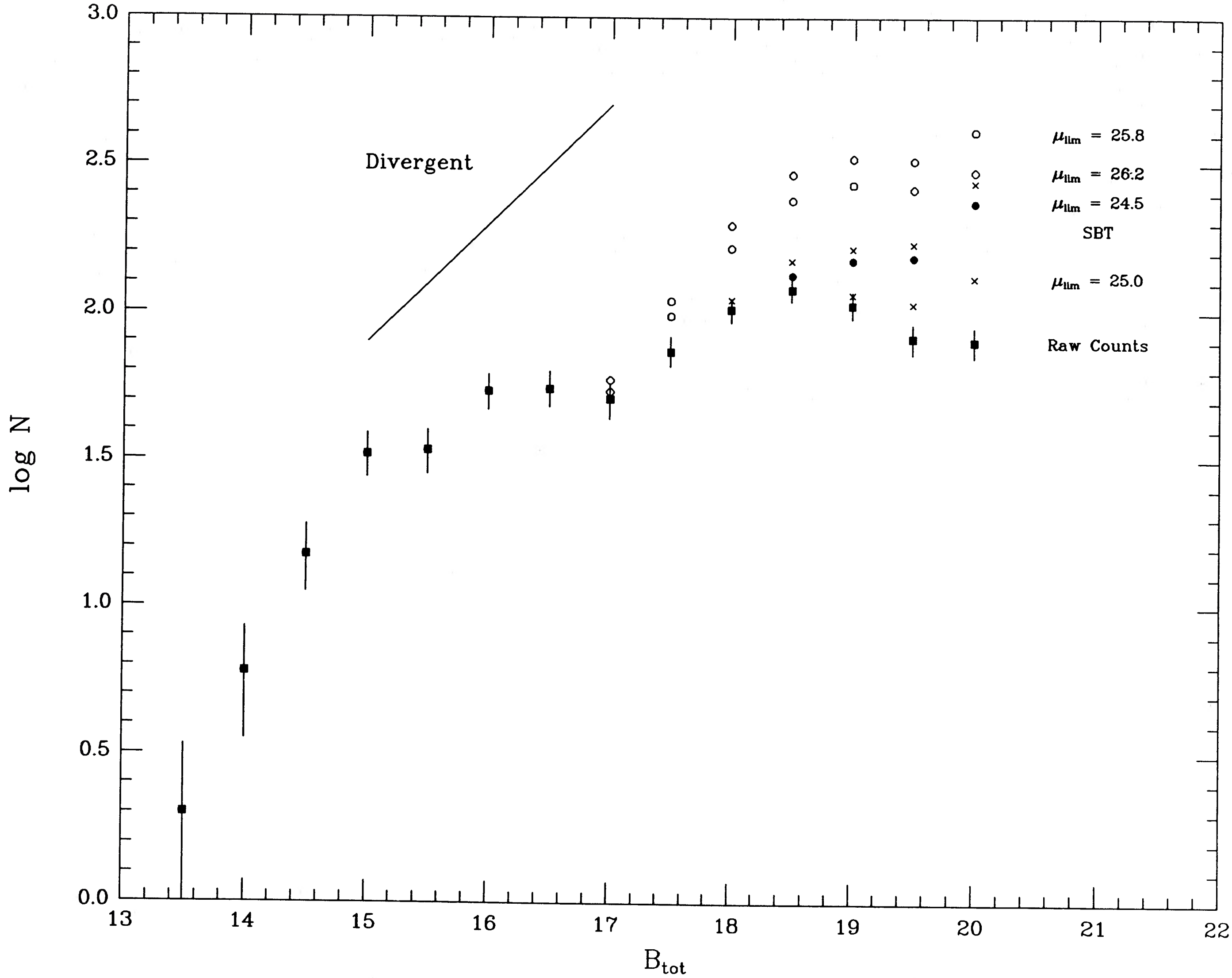

FIG. 10.—Dwarf elliptical luminosity function for the Virgo Cluster. The filled squares and circles are the raw and corrected counts from Sandage, Binggeli, and Tammann (1985), the crosses represent dwarf samples, with the incompleteness correction defined in the μ_0 vs. B_{tot} plane, and the open circles represent the same correction applied when the data from this study are included.

objects of a luminosity and surface brightness that gives them the maximum angular size on the discovery material. There may be large populations of extremely low surface brightness galaxies. Low luminosity galaxies tend to have flat cores and no nuclei. Both of these trends constitute a strong selection effect against the discovery of dwarf galaxies.

7. The uncertainty in the luminosity function of dwarf galaxies is large. The existence of large angular size, low surface brightness objects leads not only to a large correction on the observed galaxy counts, but to a brighter completeness limit for existing samples. An exponential tail to the luminosity function that would represent mass divergence (for M/L independent of L) cannot yet be ruled out.

This project would not have been possible without the high-quality plate material and fast service provided by the UK Schmidt Units at Edinburgh and Siding Spring. We acknowledge expert telescope operating and timely infusions of Milo from Angel Guerra and Fernando Peralta at the Las Campanas 100 inch telescope. We also thank the technical staff at Arecibo for excellent assistance. Conversations with Nelson Caldwell and Jeremy Mould have been very illuminating. The influence of Mike Disney on this work is gratefully acknowledged. We thank the referee for helpful comments. This research was partly supported by NSF grant INT-8600806. C. D. I. thanks Bev Oke for travel support and Caltech for a Weingart Fellowship. G. D. B. thanks Caltech for the award of a Bantrell Fellowship. D. F. M. is grateful to the staff of the UK Schmidt telescope for continuing access to first-class plate material.

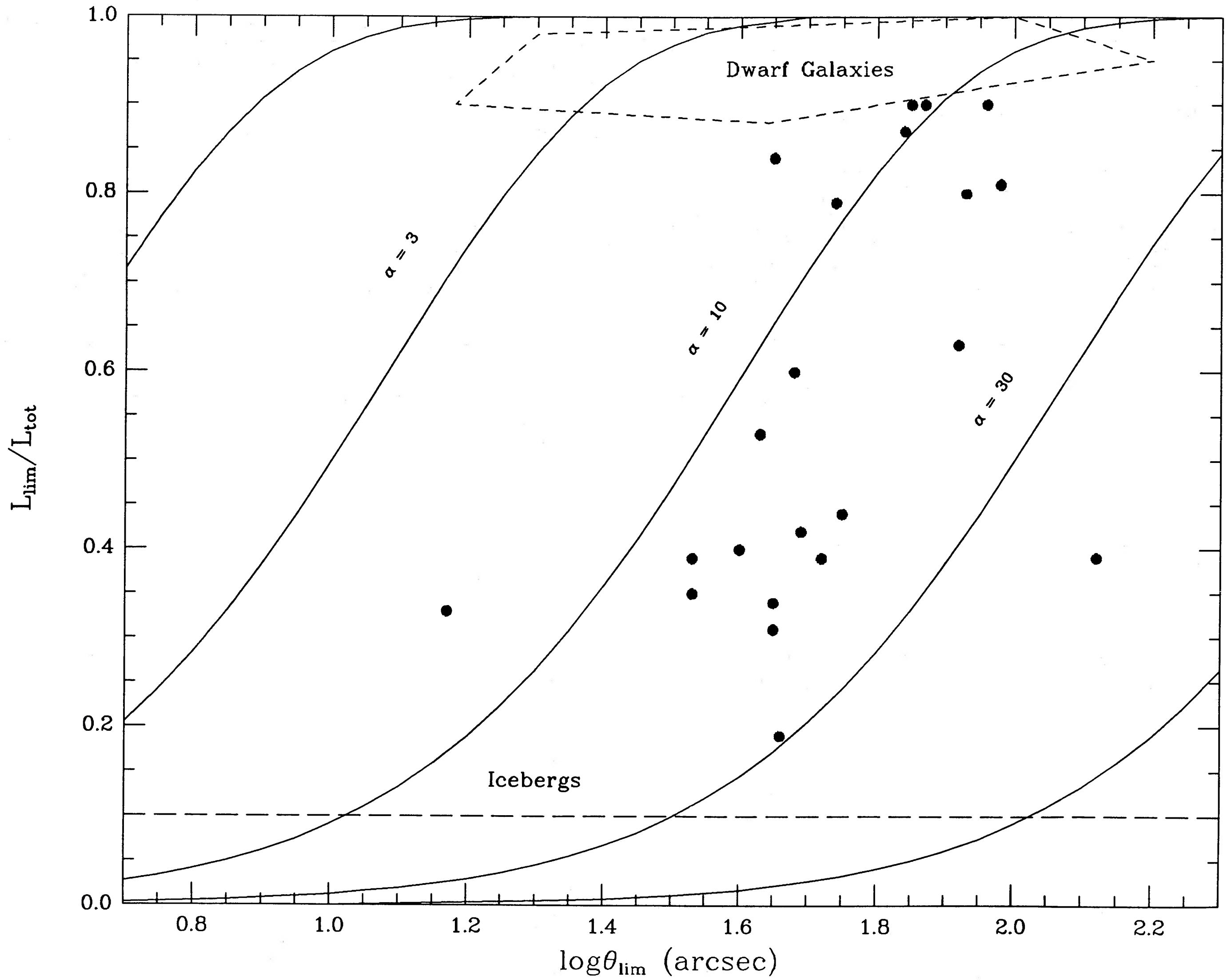

FIG. 11.—The fraction of total galaxy luminosity projecting above the $\mu_B = 27$ mag arcsec^{-2} limiting isophote plotted against angular diameter at the limiting isophote. Tracks of exponential scale length are included. The dashed box outlines the area covered by previous dwarf samples, and the new low surface brightness dwarf are plotted as filled circles.

APPENDIX

STRUCTURAL PROPERTIES OF DWARF GALAXIES

The general fitting law for the radial profiles of galaxies is

$$\ln \sigma_r = \ln \sigma_0 - (r/\alpha)^{1/\beta} , \tag{1}$$

where $\beta = 1$ for dE's and spiral disks, $\beta = 4$ for ellipticals and spiral bulges, and σ_0 and σ_r are in intensity surface brightness units. If dE galaxies are fitted by exponential profiles, described by μ_0 and α, then

$$\alpha = \left(\frac{1.086r}{\mu_r - \mu_0}\right) , \tag{2}$$

where μ_0 and μ_r are in magnitudes per square arc second. The magnitude integrated out to a radius r is

$$m_r = m_{\text{tot}} - 2.5 \log_{10} \left[1 - e^{-r/\alpha}\left(\frac{r}{\alpha} + 1\right)\right] , \tag{3}$$

and the total magnitude integrated out to infinity is

$$m_{\rm tot} = \mu_0 - 2.5 \log_{10} (2\pi\alpha^2) . \tag{4}$$

The radius containing half the light is given by

$$r_e = 1.678\alpha , \tag{5}$$

and the effective surface brightness within r_e is

$$\sigma_e = \left[\frac{(\mu_0 + 0.75 - 2.5 \log_{10} 2\pi\alpha^2)}{5.63\pi\alpha^2}\right] \tag{6}$$

Galaxy selection is usually limited to some fraction of the night sky brightness, $\mu_{\rm lim}$, corresponding to a radius in arc seconds

$$r_{\rm lim} = \left(\frac{\alpha}{1.086}\right)(\mu_{\rm lim} - \mu_0) . \tag{7}$$

As described by Allen and Shu (1979), the limiting angular diameter for constant luminosity and $\mu_{\rm lim}$ is given in arc seconds by

$$\theta_{\rm lim} = 0.735(\mu_{\rm lim} - \mu_0)10^{0.2(\mu_0 - m_{\rm tot})} , \tag{8}$$

which gives a maximum value of $\theta_{\rm lim}$ when

$$\mu_{\rm lim} - \mu_0 = 2.17 . \tag{9}$$

The fraction of the galaxy luminosity lying above the limiting isophote at $r_{\rm lim}$ is

$$\left(\frac{L_{\rm lim}}{L_{\rm tot}}\right) = \left[1 - e^{-r_{\rm lim}/\alpha}\left(\frac{r_{\rm lim}}{\alpha} + 1\right)\right] \tag{10}$$

and is plotted in Figure 11. To define an "iceberg" galaxy, we choose $\mu_{\rm lim} \approx 27$ mag arcsec^{-2}. For a given $\theta_{\rm lim}$, the galaxy is increasingly submerged below the sky brightness as μ_0 decreases. In terms of total luminosity

$$m_{\rm tot} = \mu_0 + 5 \log_{10} \left[\left(\frac{0.735}{\theta_{\rm lim}}\right)(\mu_{\rm lim} - \mu_0)\right] \tag{11}$$

giving the tracks plotted in Figure 5. This can be rearranged to produce the tracks in Figures 6 and 7. For the boundary where a galaxy can be spatially resolved in Figure 7, we note that an image with a Gaussian profile has $\alpha \approx 1.7\sigma_{\rm FWHM}$.

REFERENCES

Aaronson, M., and Olszewski, E. 1985, in *IAU Symposium 177, Dark Matter in the Universe*, ed. J. Kormendy and G. R. Knapp (Dordrecht: Reidel), p. 153.
Allen, R. J., and Shu, F. H. 1979, *Ap. J.*, **277**, 67.
Arp, H. C. 1965, *Ap. J.*, **142**, 402.
Binggeli, B., Sandage, A., and Tarenghi, M. 1984, *A.J.*, **89**, 64 (BST84).
———. 1985, *A.J.*, **90**, 1681 (BST85).
———. 1987, *A.J.*, **94**, 251.
Bothun, G. D., Impey, C. D., Malin, D. F., and Mould, J. R. 1987, *A.J.*, **94**, 23.
Bothun, G. D., and Mould, J. R. 1988, *Ap. J.*, **324**, 123.
Bothun, G. D., Mould, J. R., Caldwell, N., and MacGillivray, H. T. 1986, *A.J.*, **92**, 1007.
Bothun, G. D., Mould, J. R., Wirth, A., and Caldwell, N. 1985, *A.J.*, **90**, 697.
Caldwell, N. 1983, *A.J.*, **88**, 804 (C).
Caldwell, N., and Bothun, G. D. 1987, *A.J.*, **94**, 1126.
Cawson, M. 1983, Ph.D. thesis, University of Cambridge.
Dekel, A., and Silk, J. 1986, *Ap. J.*, **303**, 39.
Disney, M. J. 1976, *Nature*, **263**, 573.
———. 1980, in *ESO/ESA Workshop on Dwarf Galaxies*, ed. M. Tarenghi and K. Kjar (Geneva: ESO/ESA), p. 151.
Dube, R. R., Wickes, W. C., and Wilkinson, D. T. 1977, *Ap. J.* (*Letters*), **215**, L51.
Faber, S. M., and Lin, D. N. C. 1983, *Ap. J.* (*Letters*), **266**, L17.
Freeman, K. C. 1970, *Ap. J.*, **160**, 811.
Hanes, D. A., and Brodie, J. P. 1986, *M.N.R.A.S.*, **214**, 491.
Hesser, J. E., and Shawl, S. J. 1985, *Pub. A.S.P.*, **97**, 465.
Hoffman, G. L., Helou, G., Salpeter, E. E., Glosson, J., and Sandage, A. 1987, *Ap. J. Suppl.*, **59**, 1.
Hubble, E. 1936, *Ap. J.*, **84**, 270.
Ichikawa, S.-I., Wakamatsu, K.-I., and Okamura, S. 1986, *Ap. J. Suppl.*, **60**, 475 (IWO).
Ikeuchi, S., and Norman, C. A. 1987, *Ap. J.*, **312**, 485.
Kent, S. 1985, *Pub. A.S.P.*, **97**, 165.
Koo, D. C. 1986, *Ap. J.*, **311**, 651.
Kormendy, J. 1985, *Ap. J.*, **295**, 73.
Malin, D. F. 1978, *Nature*, **276**, 591.
———. 1981, *AAS Photo-Bull.*, No. 27, p. 4.
———. 1987, in *Proc. of the IAU Working Group on Astronomical Photography*, ed. S. Marx (Heidelberg: Springer-Verlag), in press.
Malin, D. F., and Murdin, P. A. 1984, *Colours of the Stars* (Cambridge: Cambridge University Press), Technical Appendix.
Norman, C. A., May, C., and van Albada, T. S. 1985, *Ap. J.*, **296**, 20.
Phillipps, S., and Disney, M. J. 1985, *Astr. Ap.*, **148**, 234.
Sandage, A., Binggeli, B., and Tammann, G. A. 1985, *A.J.*, **90**, 1759 (SBT85).
Schechter, P. 1976, *Ap. J.*, **203**, 297.
Tyson, A. J. 1988, preprint.
Tyson, N. D., and Scalo, J. M. 1988, preprint.
Zwicky, F. 1942, *Phys. Rev.*, **61**, 489.

G. D. BOTHUN: Department of Astronomy, Dennison Building, University of Michigan, Ann Arbor, MI 48109

C. D. IMPEY: Steward Observatory, University of Arizona, Tucson, AZ 86721

D. F. MALIN: Anglo-Australian Observatory, P.O. Box 296, Epping, NSW 2121, Australia